

1 2 9 0



UNIVERSIDADE D
COIMBRA

Raquel Alexandra Mateus Domingues

THE ROLE OF CARBON MONOXIDE ON
MODULATION OF MICROGLIAL
PHAGOCYTOSIS AS
NEUROINFLAMMATORY RESPONSE

Dissertação no âmbito do Mestrado em Investigação Biomédica, no ramo de Neurobiologia, orientada pela Doutora Ana Raquel Sarabando Santiago e co-orientada pela Doutora Helena Helena Luísa de Araujo Vieira apresentada à Faculdade de Medicina da Universidade de Coimbra

Outubro de 2021



The role of carbon monoxide on modulation of microglial phagocytosis as neuroinflammatory response

Raquel Alexandra Mateus Domingues

Dissertação de Mestrado na área científica de Investigação Biomédica orientada pela Doutora Ana Raquel Sarabando Santiago (Faculdade de Medicina da Universidade de Coimbra) e co-orientada pela Doutora Helena Luísa de Araujo Vieira (Faculdade de Ciências e Tecnologia da Universidade NOVA de Lisboa) e apresentada à Faculdade de Medicina da Universidade de Coimbra.

Outubro de 2021

Acknowledgements

Apesar deste trabalho ser a *minha* tese de mestrado, foi com o apoio e contributo de um grande número de pessoas que a sua realização e conclusão foi possível.

Antes de mais quero agradecer ao professor Henrique Girão e ao corpo docente, que fez parte do meu percurso ao longo do mestrado, pelo trabalho que desenvolveram e pelas oportunidades de aprendizagem surgiram graças a isso.

À Dra. Raquel Santiago por ter aceitado ser minha orientadora, pelos conselhos e por toda a disponibilidade e apoio prestados.

Um grande obrigada ao laboratório Cell Death and Disease que me acolheu de braços abertos e apoiou desde o primeiro dia. Um especial agradecimento à Dra. Helena Vieira, ao Nuno e à Daniela, pelo apoio moral, auxílio prestado e pelos conhecimentos transmitidos ao longo do meu percurso.

Um grande obrigada à comunidade do CEDOC, onde o espírito de entreajuda sempre se fez sentir ao longo do meu percurso na instituição. Em especial, à Dra. Otília Vieira pelos conselhos, conhecimento científico e materiais disponibilizados.

Quero agradecer também ao Dr. Carlos Romão por ter disponibilizado o elemento central desta tese – a ALF826.

Seria impensável não agradecer aos meus amigos que sempre estiveram presentes nos bons e maus momentos durante todo este percurso. Pela paciência, o apoio e os momentos de diversão propiciados durante os nossos encontros e noites de jogos.

Por fim, mas de certo não a última vez, quero agradecer aos meu pais pelo amor e apoio incondicional que me deram ao longo da vida e, em especial, durante esta fase.

Resumo

As células da microglia são as principais células imunitárias do sistema nervoso central (SNC). Como tal, estão envolvidas na regulação da inflamação e da fagocitose. A fagocitose é um mecanismo crucial através do qual a microglia elimina células mortas, elementos patogénicos, agregados proteicos e restos celulares, mantendo assim a homeostase dentro do SNC. Duma forma simplista, a fagocitose pode ser dividida em quatro fases - Reconhecimento, *Engulfment*, Tráfico/Maturação e Degradação. Os mecanismos moleculares que regem a fagocitose microglial ainda estão pouco estudados, principalmente as três últimas fases. O monóxido de carbono (CO) é produzido intracelularmente e já foi demonstrado que é capaz de exercer efeitos sobre uma ampla gama de proteínas e modular diferentes vias relacionadas com a regulação da resposta imune, prevenção da apoptose e o processo fagocítico. Além disso, o nosso laboratório já demonstrou que CO regula funções cruciais da microglia como a comunicação microglia-neurónio, nomeadamente, via secretoma. No entanto, no contexto da fagocitose microglial, há muito por descobrir sobre a capacidade modulatória do CO.

Assim, o principal objetivo desta tese foi explorar os efeitos do CO na fagocitose microglial. Ao longo deste trabalho, explorámos como o CO impacta o *engulfment* de partículas-alvos, o tráfego fagossomal e a degradação da carga fagocítica. Para o efeito, utilizámos a ALF826, uma nova molécula libertadora de CO, com molibdénio como centro metálico, desenvolvida pelo Dr. Carlos Romão da ITQB / Proterris.

Primeiro, otimizámos o protocolo de fagocitose, incubando esferas fluorescentes de látex com células BV2, com ou sem tratamento de CO, em condições inflamatórias e não inflamatórias. Posteriormente, as amostras foram fixadas e analisadas por microscopia de fluorescência. Em condições inflamatórias, a administração de CO tendeu a reduzir o aumento da eficiência fagocítica promovido por LPS. Considerando a relevância biológica da fagocitose de neurónios, e usando o nosso protocolo de fagocitose, avaliámos o *engulfment* de neurónios apoptóticos, através da observação de células vivas ao microscópio e ensaios de citometria de fluxo. No primeiro caso, num contexto inflamatório, o tratamento com CO não produziu efeitos significativos. No entanto, quando analisado por citometria de fluxo, o CO, tanto em

condições não inflamatórias como inflamatórias, promoveu o *engulfment* de detritos neuronais. Em seguida, a co-localização de proteínas LAMP-1 com detritos neuronais foi avaliada via microscopia confocal, como forma de avaliar o sucesso do tráfico de fagossomas para os lisossomas. O papel desempenhado pelo CO nesta fase é incerto, porém, os resultados revelaram que a sua administração influencia o tráfico de fagossomas. Usando DQ-BSA, uma proteína fluorescente *self-quenched*, avaliámos a capacidade degradativa dos fagolisossomas pela leitura da fluorescência resultante do DQ-BSA degradado e, portanto, *unquenched*. No geral, o CO promoveu a degradação da carga fagocítica, em condições não inflamatórias.

Em suma, a administração de CO promove o *engulfment* de neurónios mortos por parte da microglia. Por forma a poder-se tirar conclusões mais definitivas e averiguar o impacto concreto do CO nas fases de tráfico e de degradação, é necessária a realização de mais experiências.

Palavras-chave: monóxido de carbono, microglia, fagocitose, neurónios, inflamação

Abstract

Microglia are the primary resident immune cells of the central nervous system (CNS). As such, they are involved in the modulation of inflammation and phagocytosis. Phagocytosis is a crucial mechanism through which microglia are able to clear dead cells, pathogens, protein aggregates and cellular debris, thus contributing to CNS's homeostasis maintenance. From a simplistic view, phagocytosis can be divided into four stages – Recognition, Engulfment, Trafficking/Maturation and Degradation. The molecular mechanisms behind microglial phagocytosis are still poorly understood, especially the last three stages. Carbon monoxide (CO) is produced intracellularly and has been shown to exert effects on a wide range of proteins and modulating different pathways related to immune response regulation, apoptosis prevention and the phagocytic process. Furthermore, our lab as already disclosed that CO regulates crucial microglial functions related to microglia-neuron communication, in particular via secretome. However, in the context of microglial phagocytosis, there is much to uncover about CO's modulation capability.

Thus, the main goal of this thesis was to explore CO's effects on microglial phagocytosis. Throughout this work we explored how CO impacts target engulfment, phagosomal trafficking and cargo degradation. We used the novel molybdenum-based CO-releasing molecules ALF826 developed by Dr. Carlos Romão from ITQB/Proterris.

Firstly, we optimized the phagocytosis protocol by incubating fluorescent latex beads with BV2 cells, with or without CO treatment, under inflammatory and non-inflammatory conditions. Samples were later fixed and analysed through fluorescence microscopy. Under inflammatory conditions, CO administration tended to reduce the increase in phagocytic efficiency promoted by LPS. Considering the biological relevancy of microglial neuronal clearance and using our phagocytosis protocol, we assessed the engulfment of apoptotic neurons through live cell imaging and flow cytometry assays. In the former, application of CO did not produce significant effects under an inflammatory context. However, when analysed through flow cytometry, CO, under both non-inflammatory and inflammatory conditions, promoted neuronal debris engulfment by almost 1-fold in comparison to the controls. Subsequently, co-localization of LAMP-1 proteins with neuronal debris was assessed through confocal

microscopy, as a means of evaluating the trafficking of phagosomes into lysosomes. The role played by CO at this stage is uncertain, however, the results revealed that its administration influences phagosomal trafficking. Using DQ-BSA, a self-quenched fluorescent protein, we evaluated the degradative capacity of phagolysosomes by reading the resulting fluorescence from degraded, and thus unquenched, DQ-BSA. Overall, CO promoted cargo degradation in non-inflammatory conditions.

In summary, CO administration promotes neuronal debris engulfment by microglia. Further experiments are required so as to draw more definite conclusions and better define CO's impact on the trafficking and degradation stages.

Keywords: carbon monoxide; microglia; phagocytosis; inflammation; neurons

Table of Contents

Acknowledgements	III
Resumo.....	V
Abstract	VII
List of figures	X
List of tables.....	X
List of abbreviations	XI
Chapter 1 - Introduction	13
1.1. A brief view of the history of neuroscience	15
1.2. Cell typology.....	17
1.2.1. Neurons.....	17
1.2.2. Glial cells.....	18
1.3. Microglia: neuroinflammation and microglial inflammatory response	21
1.3.1. Microglial phagocytosis	23
1.4. Haem oxygenase and haem degradation products	29
1.5. Carbon Monoxide.....	32
1.5.1. Molecular targets underlying CO's biological functions	33
1.5.2. Therapeutical potential of CO and the use of CO-releasing molecules	34
1.6. The role of carbon monoxide in mediating microglial immune response	39
1.7. Final remarks and objectives	41
Chapter 2 – Materials and methods	43
2.1. Cell cultures	45
2.1.1. BV2 cell line.....	45
2.1.2. CAD cell line.....	45
2.2. ALF826 preparation	45
2.3. Bead engulfment assays.....	46
2.4. DQ-BSA degradation assays.....	49
2.5. Neuron engulfment assays	50
2.5.1. Live imaging.....	52
2.5.2. Flow cytometry	52
2.6. Lysosomal-associated membrane protein-I localization assessment	52
2.7. Statistical Analysis.....	53
Chapter 3 – Results	55
3.1. Engulfment stage.....	57
3.1.1. Phagocytosis protocol optimization: bead engulfment assays	57
3.1.2. Phagocytosis protocol: apoptotic neuron engulfment assays	61
Live imaging.....	61
Flow cytometry	63
3.2. Trafficking/Maturation stage	65
3.2.1. Phagocytosis protocol: LAMP-I co-localization assessment	65
3.3. Degradation stage.....	67
3.3.1. Phagocytosis protocol: degradative function assessment	67
Chapter 4 – Discussion.....	69
4.1. Engulfment stage	72
4.1.1. Phagocytosis protocol optimization (beads)	72
4.1.2. Phagocytosis protocol (apoptotic neurons)	73
4.2. Trafficking/maturation stage.....	75
4.3. Degradation stage.....	77
4.3.1. Phagocytosis protocol (DQ-BSA)	77
4.4. Final remarks	77
Chapter 5 – Conclusion.....	81
References	85

List of figures

<i>Figure 1</i> – Types of neuronal morphology.....	17
<i>Figure 2</i> – The basis of a neuronal network.	18
<i>Figure 3</i> – Glial cells in the central nervous system.	19
<i>Figure 4</i> – Microglial immune response model.....	22
<i>Figure 5</i> – Microglial phagocytosis model.	24
<i>Figure 6</i> – Receptor/signal pairings in microglia and neuron interactions during phagocytosis.	25
<i>Figure 7</i> – LC3-associated phagocytosis in comparison with autophagy process.	28
<i>Figure 8</i> – Haem degradation reaction.	30
<i>Figure 9</i> – Carbon monoxide’s effect on microglial function.	39
<i>Figure 10</i> – Main questions aimed to answer in this thesis.	42
<i>Figure 11</i> – Bead engulfment assay following protocol A (optimization).	58
<i>Figure 12</i> – Bead engulfment assays following protocol B (optimization).....	59
<i>Figure 13</i> – Bead engulfment assays following protocol B.....	60
<i>Figure 14</i> – Neuronal debris engulfment assays (optimization) – live imaging.	62
<i>Figure 15</i> – Neuronal debris engulfment assays – live imaging.	63
<i>Figure 16</i> – Gating model utilized during flow cytometry assays.....	64
<i>Figure 17</i> – Neuronal debris engulfment assays – flow cytometry.	65
<i>Figure 18</i> – LAMP-1 co-localization assays.....	66
<i>Figure 19</i> – DQ-BSA degradation assays.....	68
<i>Figure 20</i> – Main conclusions from this thesis.....	83

List of tables

<i>Table 1</i> – Key events in neuroscience.....	15
<i>Table 2</i> – Catalytic haem oxygenase isoforms.....	31
<i>Table 3</i> – CORMs.....	35
<i>Table 4</i> – Effects associated with CO application.	36
<i>Table 5</i> – Assays conducted according to protocol B.....	48
<i>Table 6</i> – Degradative capacity protocol.	49
<i>Table 7</i> – Protocol used to study neuronal debris phagocytosis.....	51

List of abbreviations

AD	Alzheimer's Disease
ADP	Adenosine diphosphate
AF	Alexa fluor
ATP	Adenosine 5'-triphosphate
Aβ	Amyloid beta
BR	Bilirubin
BSA	Bovine serum albumin
BV	Biliverdin
CNS	Central nervous system
CO	Carbon monoxide
CORMs	CO-releasing molecules
COX	Cytochrome c oxidase
DAMPs	Damage-associated molecular patterns
DMEM/F12	Dulbecco's Modified Eagle Medium/F12
DMSO	Dimethyl sulfoxide
FBS	Fetal bovine serum
FSC	Forward scatter
Gas-6	Growth arrest-specific 6
GPR56	G protein-coupled receptor
H₂O₂	Hydrogen peroxide
HIF-1α	Hypoxia-inducible factor-1 α
HO	Haem oxygenase
IB4	Isolectin B-4
IFN-γ	Interferon- γ
IL	Interleukin
iNOS	Nitric oxide synthase
LAMP-1	Lysosomal-associated membrane protein-1
LANDO	LC3-associated endocytosis
LAP	Microtubule-associated protein 1A/1B-light chain 3-dependent phagocytosis
LC3	Microtubule-associated protein 1A/1B-light chain 3
LPS	Lipopolysaccharide
MAMPs	Microbe-associated molecular patterns
MAPK	Mitogen-activated protein kinases

MerTK	MER Receptor Tyrosine Kinase
MFG-E8	Milk fat globule-EGF factor 8
MW	Multi-well
NF-κB	Nuclear factor-κB
NO	Nitric Oxide
NOX2	NADPH oxidase 2
NRF	Nuclear respiratory factor
NS	Nervous system
PBS	Phosphate buffered saline
PFA	Paraformaldehyde
PI3KC3	Phosphatidylinositol 3-kinase
PIP3	Phosphatidylinositol 3-phosphate
PNS	Peripheral nervous system
PPARγ	Peroxisome proliferator- activated receptor γ
PtdSer	Phosphatidylserine
rcf	Relative centrifugal force
ROS	Reactive oxygen species
sGC	Soluble guanylate cyclase
Siglec	Sialic acid-binding immunoglobulin-type lectin
SIRPα	Signal-regulatory protein α
SSC	Side scatter
TAMRA	5-(and-6)-carboxytetramethylrhodamine succinimidyl ester
t-BHP	<i>tert</i> -butyl hydroperoxide
TFAM	Mitochondrial transcription factor A
TLR	Toll-like receptors
TNF-α	Tumour necrosis factor- α
TREM2	Triggering receptor expressed on myeloid cells 2
UVRAG	UV radiation resistance-associated gene
VNR	Vitronectin receptor
VPS	Vacuolar protein sorting

Chapter I

Introduction

Chapter I – Introduction

I.1. A brief view of the history of neuroscience

Our everyday lives require the performance of a plethora of tasks, each one with a varying degree of complexity. We give little to no thought at the diverse and intricate neuronal mechanisms that dictate their feasibility and efficiency. Neuroscience is the scientific study of the nervous system (NS). The questions posed in this line of study rely heavily on the output of several disciplines like physiology, biochemistry, genetics, immunology and mathematics in order to reach the answers.

From very early in our history, we have shown great interest in studying the NS. A document written in 1700 BC by the Egyptian physician Imhotep is prime evidence of this. Despite part of it missing, this manuscript describes 48 cases of brain injuries alongside with the examination process and the treatment applied ¹. In Ancient Greece, Hippocrates was aware of many of what are now valid concepts in neurology ². His observations and ideas on neurological diseases like apoplexy, spondylitis, hemiplegia, and paraplegia pioneered modern day neurology. Hippocratic medicine was detailed in a collection of 72 treatises kept in the library of Alexandria.

Throughout the 19th – 20th century period, many experiments and key events, not only fomented the scientific community's interest in neuroscience, but also generated valuable insights into neuronal biology and function and cerebral pathologies. Some of those events are described in *Table 1*.

Table 1 – Key events in neuroscience. This table displays a chronological order (top to bottom) of some discoveries and experiments, conducted throughout the 19th – 20th century period, that shaped our current neuroscientific knowledge. Adapted from the chronology in ref. ³.

Date	Event	Ref.
1837	Jan Purkyně describes Purkinje cells – large neurons with many branching dendrites found in the cerebellum.	[3]
1843	Emil du Bois-Reymond demonstrates the electrical nature of the nerve signal.	[4]
1858	Rudolph Virchow coins the term neuroglia.	[5]
1891	Heinrich Wilhelm Gottfried von Waldeyer-Hartz proposes the term neuron	[6]

Table 1 (cont.) – Key events in neuroscience. This table displays a chronological order (top to bottom) of some discoveries and experiments, conducted throughout the 19th – 20th century period, that shaped our current neuroscientific knowledge. Adapted from the chronology in ref. 3.

Date	Event	Ref.
1891	Mihaly Lenhossék describes a star-shaped cell population in the central nervous system, introducing the term astrocyte.	[5]
1897	Heinrick Quincke performs lumbar puncture to study cerebrospinal fluid.	[7]
1906	Charles Scott Sherrington coins the term synapse.	[7]
1907	Golgi and Ramón y Cajal wins the Nobel Prize in Physiology or Medicine for their extensive observations, descriptions, and categorizations of neurons in the brain.	[3]
1919	John Newport Langley introduces the concept of receptor molecules.	[3]
1921	Pío del Río Hortega describes microglia.	[3]
1927	Pío del Río Hortega describes oligodendrocytes (oligodendroglia).	[3]
1927	Julius Wagner-Jauregg receives the Nobel Prize in Physiology or Medicine for treating dementia paralyse (caused by neurosyphilis) with malaria inoculation.	[3]
1932	Edgar Douglas Adrian and Charles S. Sherrington share the Nobel Prize in Physiology or Medicine for work on the function of neurons (studies on electrical signals in the nervous system and spinal cord and brain process nerve impulses, respectively).	[3]
1938	Franz Kallmann publishes <i>The Genetics of Schizophrenia</i> .	[3]
1949	Egas Moniz receives the Nobel Prize in Physiology or Medicine for applying leucotomy to treat certain psychoses.	[3]
1951	John Cade discovers that lithium can be used as treatment for bipolar depression.	[3]
1951	Monoamine oxidase inhibitors are introduced to treat psychotic patients.	[3]
1952	Alan Lloyd Hodgkin and Andrew Huxley present a mathematical model for transmission of electrical signals in neurons (action potentials), how they are initiated and propagated (Hodgkin–Huxley model).	[8]
1961	Levodopa successfully treats parkinsonism.	[3]
1961	Eldon Foltz performs the first cingulotomy to treat chronic pain.	[3]
1970	Julius Axelrod, Ulf Svante von Euler and Bernard Katz share the Nobel Prize in Physiology or Medicine for work on neurotransmitters (studies on noradrenaline, norepinephrine and their transmissions through synapses, respectively).	[3]
1972	Jennifer and Matthew LaVail use horseradish peroxidase to study axonal transport.	[3]
1973	Sinemet is introduced as a treatment for Parkinson's disease.	[3]
1974	M. E. Phelps, E. J. Hoffman and M. M. Ter-Pogossian develop the first PET scanner.	[3]
1993	The gene responsible for Huntington's disease is identified.	[3]
1997	Stanley B. Prusiner receives the Nobel Prize in Physiology or Medicine for the discovery of prions.	[3]
1998	First evidence of neurogenesis in the hippocampus of adult human samples was reported.	[9]
2000	Arvid Carlsson, Paul Greengard and Eric Kandel share the Nobel Prize in Physiology or Medicine for their discoveries concerning signal transduction in the nervous system (discovery of dopamine, studies on how several different signal substances work and the discovery that chemical signals changed the structure of the connections between cells, respectively).	[3]

1.2. Cell typology

The NS is divided into the central (CNS) - brain and spinal cord - and the peripheral NS (PNS) – nerves – which connects the former to the rest of the body. The cells that compose these systems and/or help maintain their function are generally categorized as neurons and glial cells.

1.2.1. Neurons

Both the CNS and PNS are comprised of billions of neurons. Through a series of elaborate networks, neurons are able to encode, transmit and store information we receive from internal and external stimuli. Neurons possess a very unique anatomy in comparison to other cells. Based on their morphology, neurons can be classified into multipolar, bipolar, pseudo-unipolar, and anaxonic (*Figure 1*)¹⁰. Their structure can be divided into three sections – dendrites, soma, and the axon (*Figure 2A*)¹¹. Neuron morphology classification varies primarily in their arrangement and number of axons and dendrites¹⁰.

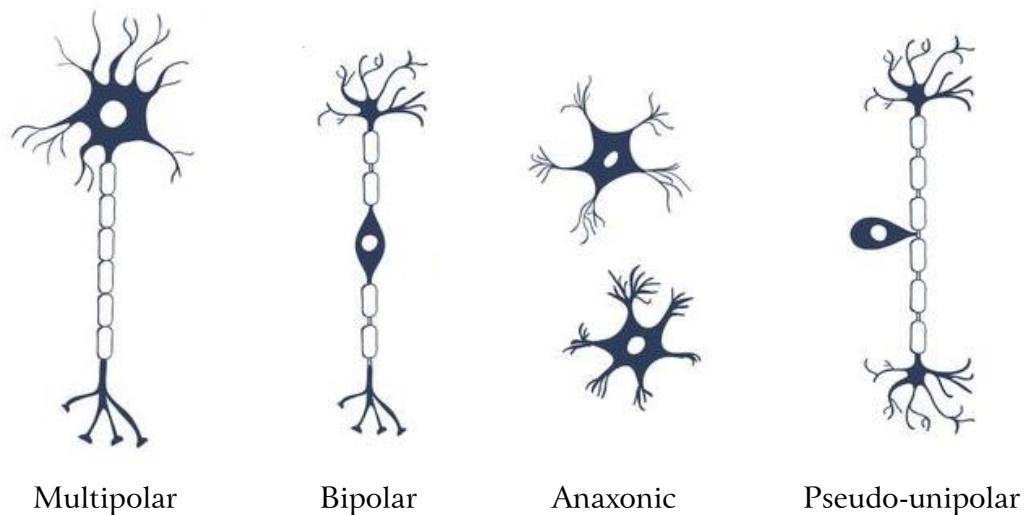


Figure 1 – Types of neuronal morphology. This image serves as a representation of the diverse morphology neurons can have. These cells can be multipolar, bipolar, anaxonic or pseudo-unipolar. Adapted from: <https://www.vecteezy.com/vector-art/115820-neuron-vector>.

Synapse contacts, in the CNS, occur between pre-synaptic neuron's axon terminal and the post-synaptic neuron's dendrites or, although less frequently, cell body. There are two types of synapses – chemical (*Figure 2C*) and electrical synapses

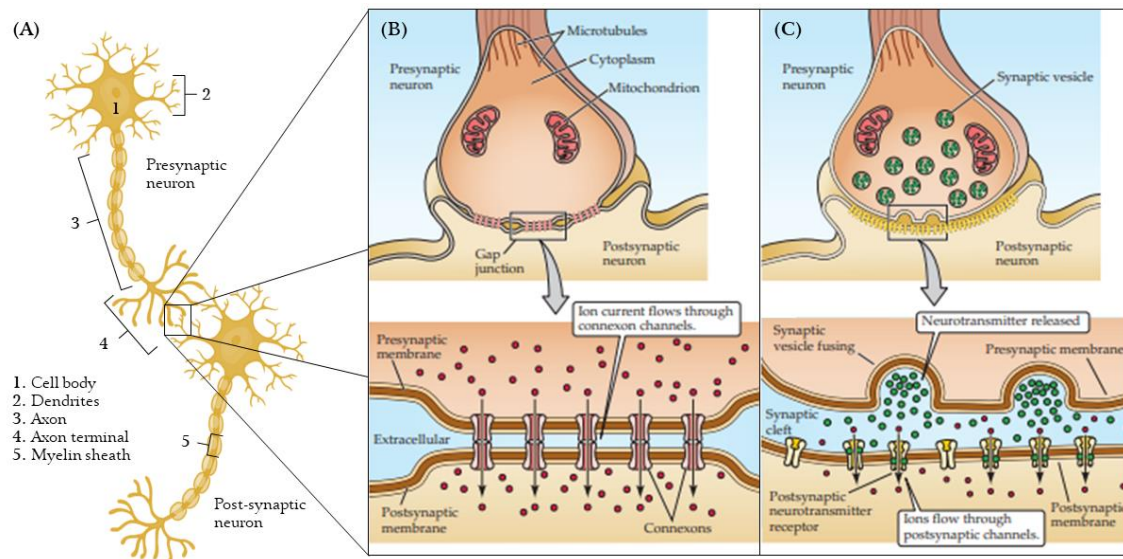


Figure 2 – The basis of a neuronal network. (A) The basic structure of neurons. Adapted from <https://www.pngkey.com/maxpic/u2r5o0u2y3i1a9w7/>. (B, C) Electrical and chemical synapse, respectively. Adapted from: Purves (2018) ISBN: 978-1-60535-380-7.

(Figure 2B) ¹¹. At chemical synapses, the passage of the signal happens through the secretion of specialized molecules – neurotransmitters - into the synaptic cleft, that will bind to specific receptors exposed on the post-synaptic neuron’s membrane. Neurotransmitters travel through the axon inside synaptic vesicles. They range from gaseous molecules (e.g., nitric oxide (NO)) to more complex chemical structures (e.g., endorphin). In terms of function, they can be excitatory (e.g., acetylcholine), inhibitory (e.g., serotonin) or both (e.g., dopamine). Once they reach the axon’s terminal, the vesicles fuse with the membrane releasing their contents into the synaptic cleft. Upon binding to their respective receptors, these molecules modify the electrical properties of the post-synaptic cell, allowing for signal propagation (Figure 2B). On the other hand, electrical synapses allow for the passive flow of electrical current. This current is generated by the action potential in the presynaptic neuron. At the contact site, specialized structures – connexons – provide passage for the electrical signal.

1.2.2. Glial cells

In the 19th century, thanks to the work of Rudolph Virchow, Santiago Ramón y Cajal, Pio del Río-Hortega and others, glial cells were discovered. *Neuroglia* was a term first introduced by Rudolph Virchow in 1858 to describe this group. Initially, it

was proposed that neuroglia's role was entirely passive, serving only to fill the space not occupied by neurons and only to physically support them. Throughout the second half of the 19th century, many different forms of glial cells were documented by scientists. Glial cells can be divided into three major groups – astrocytes, oligodendrocytes and microglia (*Figure 3*).

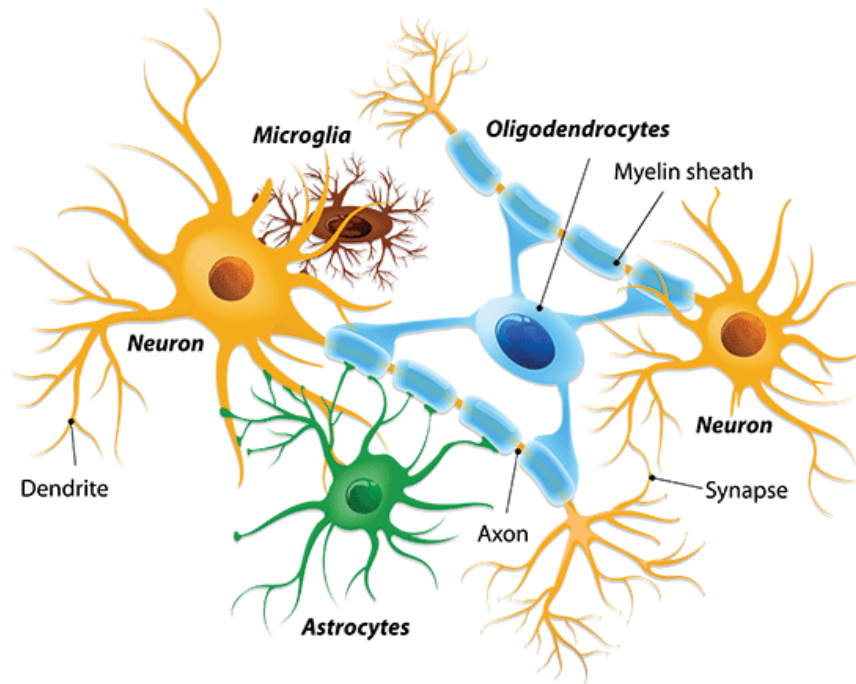


Figure 3 – Glial cells in the central nervous system. Depiction of an astrocyte, oligodendrocyte and a microglial cell interacting with neurons. Source: ID 47546395 © Designua | Dreamstime.com

Astrocytes

In 1895, Mihaly von Lenhossék described a star-shaped cell population in the CNS, thus introducing the term astrocyte. These cells are found to be spread throughout the brain. Their branch-like extensions are often seen in close contact with nerve terminals, allowing for an active astrocyte-neuron communication through the synaptic clefts ¹². They execute important functions like managing the glutamine/glutamate cycle ¹³, providing neurons with glutathione and glutathione precursors ¹⁴ as well as lactate as source of carbon ¹⁵. They supply neurons with nutrients ¹⁶, by acting as intermediates between blood vessels and neurons. Studies have shown that astrocytes influence the number of synapses a neuron can form during development ¹⁷. Moreover, they have influence over neuron activity through Ca^{2+} modulation ¹⁸⁻²⁰ and neurotransmitters uptake ²¹. As a response to inflammation and/or injury, astrocytes are known to become reactive ²², altering their homeostatic

functions like potassium ion uptake, ion buffering, Ca^{2+} signalling, and excitatory neurotransmitter uptake.

Oligodendrocytes

Pío del Río Hortega first described oligodendrocytes in a series of three papers published in 1921, 1922 and 1928²³. These cells' major function is to generate myelin, through extension of their cell membrane and wrapping it tightly around axons in order to facilitate signal transmission throughout long distances.

Microglia

Microglia are often described as being the CNS's resident immune cells. Pío del Río Hortega, in a series of four papers (all published in 1919), presented the protocol that was used to specifically stain microglia, described their general morphology in normal and pathological states and he characterized some functional features, like their high migration and phagocytic rates in pathological conditions²³.

Microglia have several functions, namely, orchestration of immune responses in order to protect and maintain neuronal homeostasis. Moreover, they also phagocytize cellular debris²⁴ and living cells throughout brain development²⁵ and during pathological situations²⁶, as well as post-natal synaptic pruning²⁷ for synaptic plasticity management²⁸. Microglia are able to recognize pathogens and microenvironmental changes through surface receptors that are able to detect complement fragments, immunoglobulins, adhesion molecules, chemokine, scavenger, Fc and Toll-like receptors (TLR) and purinoreceptors²⁹. Upon encountering such stimuli, microglia shift from a “resting” state to an “active” one, becoming ameboid and increasingly proliferative. While in a “resting” state, microglia possess a dynamic and ramified morphology. Studies have reported that the cell body of resting microglia have essentially no movement at all. However, their extensions were shown to have highly motile extension and retraction processes. This allows them to quickly scan the extracellular space, in a random, but dynamic and highly efficient fashion^{30,31}.

1.3. Microglia: neuroinflammation and microglial inflammatory response

Depending on the initial activating stimuli and surrounding environment, microglia are phenotypically heterogeneous, ranging from more pro-inflammatory phenotypes to anti-inflammatory phenotypes. The nomenclature utilized for macrophages is often applied to microglia. Phenotypes are varied and have been expanded from the classical binary and fixed view of M1 (pro-inflammatory) and M2 (anti-inflammatory), to be viewed as multidimensional^{32,33}. In other words, an individual microglial cell's phenotype is transient, meaning it fluctuates between more anti-inflammatory or more pro-inflammatory temporally and spatially, depending on the initial activating stimulus and its current surrounding microenvironment.

Neuroinflammation is the triggering of an immune response within the nervous tissue. The triggering stimuli might come from aseptic or non-aseptic insults (e.g., mechanical injury and infections, respectively)³⁴. Microglial cells are crucial players in this process (*Figure 4*). Upon injury and/or infection, microglia are able to identify microbe-associated molecular patterns (MAMPs) (e.g., lipopolysaccharide (LPS)) and/or damage-associated molecular patterns (DAMPs) (e.g., adenosine 5'-triphosphate (ATP)) and develop a more pro-inflammatory phenotype. Normally, these include the release and production of pro-inflammatory cytokines and other potentially cytotoxic factors (e.g., tumour necrosis factor- α (TNF- α), interleukin (IL)- β , NO, reactive oxygen species (ROS))³⁵⁻³⁷. However, this immune response can promote neurotoxicity due to the release of pro-inflammatory and neurotoxic factors, promoting neuronal death, which further aggravates the microenvironment, thus reinforcing the pro-inflammatory immune response. Because of this, microglia mount an anti-inflammatory response to rapidly heal and restore tissue homeostasis³⁷⁻³⁹. Understandably, neuroinflammation is required to be tightly controlled, because uncontrolled inflammatory processes can lead to neuronal damage and cognitive decline. This is thought to be a key promoter of neurodegenerative diseases progression (e.g., Alzheimer's Disease (AD)) as well as an aggravator of acute injuries (e.g., stroke).

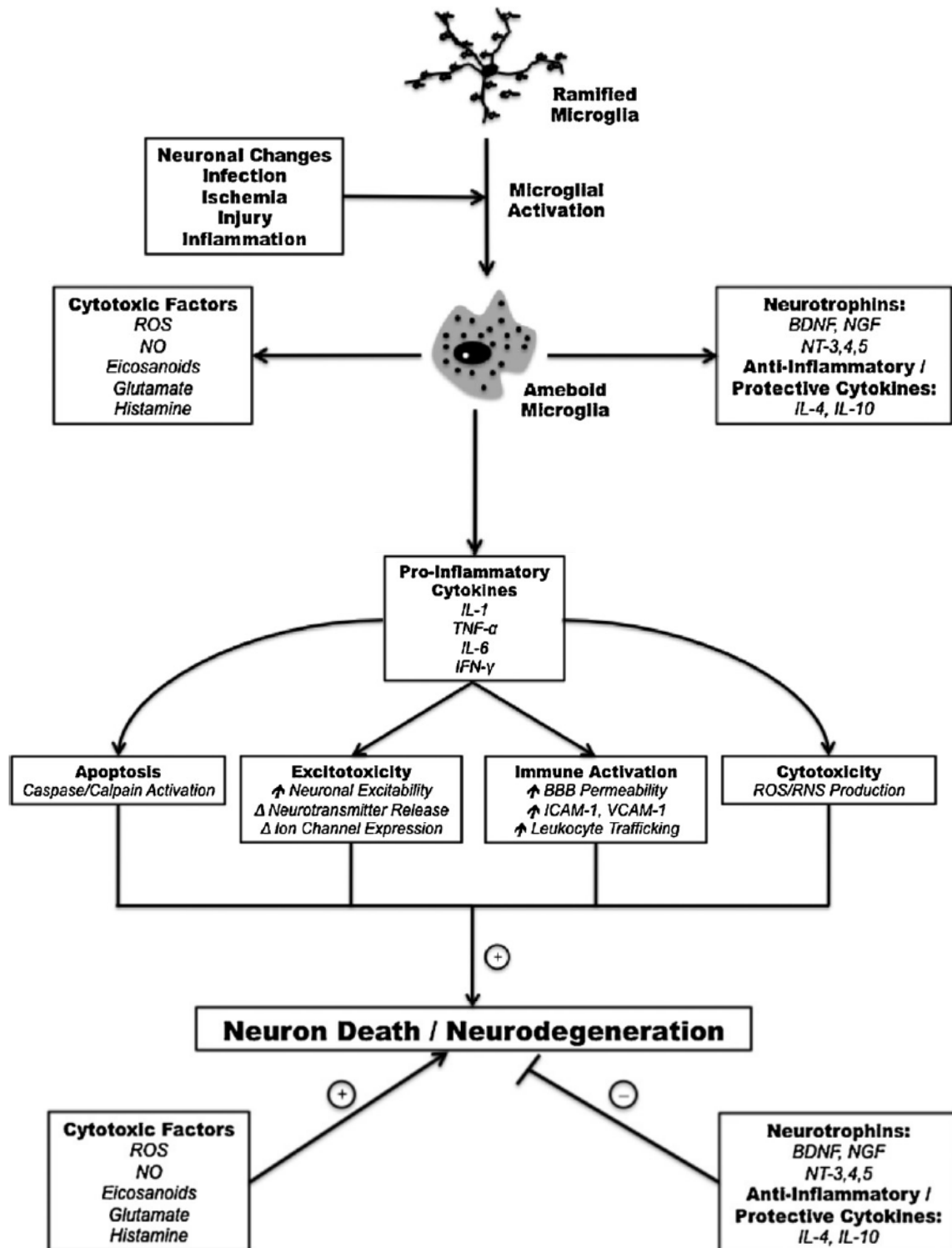


Figure 4 – Microglial immune response model. Upon encountering certain stimuli, microglia transition from the “resting” state to an “active” state. This results in the release of pro-inflammatory and anti-inflammatory cytokines and other potentially cytotoxic factors (e.g., ROS, NO, etc) as a means to resolve the initial pathological trigger. The balance between the pro-inflammatory, the anti-inflammatory response and the duration and intensity of the immune response, will dictate the extent of neuronal death/damage. Source: Smith *et al.* (2012) (doi: 10.1016/j.brainresbull.2011.10.004).

In AD, microglia increase the production of inflammatory cytokines when amyloid beta (A β) deposition increases⁴⁰. One-way A β is eliminated from the CNS is via microglial⁴¹ and astrocytic^{42,43} phagocytosis. Microglia migrate towards A β aggregates and begin to accumulate in the area surrounding the deposits. By doing this, microglia are capable of limiting A β plaque spread by isolating these deposits. Microglia's ability to phagocyte A β may depend on their phenotype. Pro-inflammatory-leaning phenotypes tend to inhibit microglial phagocytosis of A β , while anti-inflammatory-leaning phenotypes promote it^{44,45}.

Neuroinflammation is also strongly associated with ischemic and haemorrhagic stroke. Ischaemic stroke occurs when blood flow is interrupted or reduced in an area of the brain. This prevents the cells in said area from receiving oxygen and nutrients, whereas a haemorrhagic stroke is when, a blood vessel bursts, leading to internal bleeding in the brain. In both cases, a neuroinflammatory response is orchestrated in order to mitigate further damages. In case of ischaemic stroke, two regions can be defined – ischaemic core and the penumbra region. The former is composed of tissue that is already irreversibly necrotic regardless of reperfusion. The latter area surrounds the ischaemic core and is in the process of becoming necrotic but is still salvageable. This type of environment favours pro-inflammatory phenotypes⁴⁶. In addition, studies have shown that mice submitted to experimental stroke who lacked IL-4 and IL-10 (anti-inflammatory cytokines) had higher infarct volume and worse cognitive scores^{47,48}.

1.3.1. Microglial phagocytosis

Phagocytosis is the process of engulfing target particles, usually larger than 0.5 μ m, into plasma membrane-derived vesicles (phagosomes). Molecular mechanisms associated with macrophage phagocytosis have been extensively researched throughout the past years⁴⁹, but research specifically into microglial phagocytosis is still in its youth by comparison⁵⁰. So far, studies point to both processes being carried out in a very similar, if not identical, way.

MAMPs are expressed by microbes and/or pathogens (e.g., LPS), while DAMPs are often released and/or exposed by dying/stressed cells (e.g., ATP) in case of events like trauma and ischaemia⁵¹. So, phagocytes are not only responsible for the engulfment and elimination of foreign particles, microbes and pathogens, but also of clearing out apoptotic cells and cellular debris, thus contributing to tissue homeostasis. After binding to the specific receptor, extensive actin remodelling occurs in order to properly envelop the targeted particles and form the phagosome. This compartment undergoes a maturation process, leading up to fusion with lysosomal vesicles for subsequent cargo degradation. Overall, phagocytosis is a complex sequence of coordinated events, but, in a simplistic view, can be divided into four stages – Recognition, Engulfment, Trafficking/Maturation and Degradation (*Figure 5*). Like other phagocytes, microglia rely on the “find me”, “eat me/don’t eat me” signalling cues that occur between them and neurons (*Figure 6*).

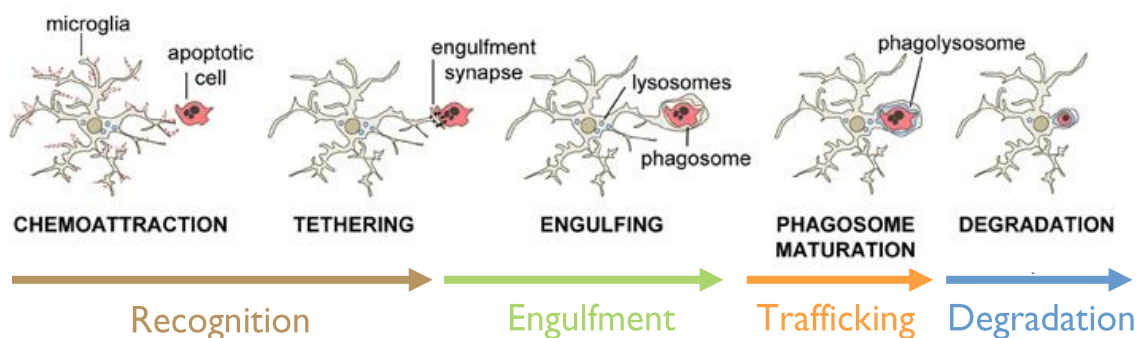


Figure 5 – Microglial phagocytosis model. This image illustrates the sequence of events throughout the occurrence of a phagocytic event by microglia.

Adapted from Sierra *et al.* (2013) (doi: 10.3389/fncel.2013.00006).

“Find me” signalling

Whether by the natural turnover process or by injury (e.g., trauma, ischaemic event), dying neurons release a variety of chemoattractant factors (e.g., ATP, adenosine diphosphate (ADP), fractalkine) that will attract phagocytic microglia. ATP and ADP are some of the most studied “find-me” signals. When ATP and/or ADP are released into the extracellular matrix, these molecules trigger P2Y receptors on the outer membrane of microglia^{52,53}.

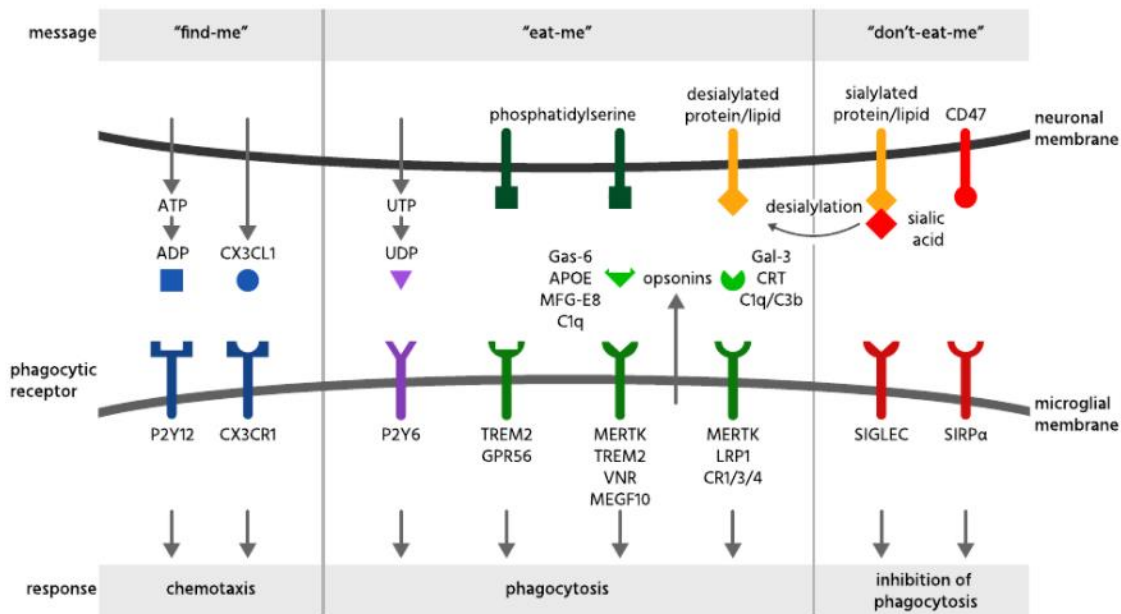


Figure 6 – Receptor/signal pairings in microglia and neuron interactions during phagocytosis.

The diagram depicts examples of pairings between receptors present on the outer membrane of microglial cells and of signals released/exposed by neurons. Each pairing is classified into one of three categories – “find me”, “eat me” or “don’t eat me” signals – and the respective response elicited by such coupling – chemotaxis towards the source of the signal, phagocytosis of target or phagocytosis blockade.

Source: Butler *et al.* (2021) (doi: 10.1111/jnc.15327).

“Eat me” signalling

In addition, stressed and/or dying neurons often expose what are known as “eat me” signals, which are recognized by somewhat specific receptors on microglia. The most studied eat me signal displayed by dying/stressed neurons is phosphatidylserine (PtdSer)⁵⁴, but desialylation of lipids/proteins on neurons’ cell surface is another example⁵⁵. Usually, PtdSer is located in the inner leaflet of the plasma membrane, and kept that way, through the activity of ATP-driven translocases. However, it can become exposed to the extracellular milieu in certain circumstances (e.g., apoptosis)^{56,57}. This can happen either reversibly, through the activity of Ca²⁺-activated PtdSer scramblases, or irreversibly by caspase-activated scramblases⁵⁷. Additionally, stressed neurons may reversibly expose PtdSer due to transient stress factors (e.g., ROS), leaving them susceptible to phagocytosis by microglia⁵⁸. Microglia are able to detect the exposed PtdSer via direct binding to specific receptors, namely, triggering receptor expressed on myeloid cells 2 (TREM2) and G protein-coupled receptor (GPR56)^{59,60}, or indirectly binding to receptors (MER Receptor Tyrosine Kinase (MerTK) vitronectin receptor (VNR)) through opsonin (e.g., growth arrest-specific 6 (Gas-6), Milk fat globule-EGF factor 8 (MFG-E8))⁶¹.

“Don’t eat me” signalling

CD47 and sialylated proteins and/or lipids on the target cell’s surface are well known “don’t eat me” signals, displayed by healthy cells. Neurons that express CD47 protect themselves from being phagocytic targets by engaging with signal-regulatory protein alpha (SIRP α) receptor expressed on microglial cell surface^{62,63}. Sialic acids present on the surface of brain cells serve as a “intact self” signal, which prevents microglia from attacking intact/healthy cells. They lead to phagocytosis inhibition by interacting with sialic acid-binding immunoglobulin-type lectin (Siglec) receptors displayed by microglia or by blocking opsonin binding, thus preventing interactions with phagocytosis-promoting receptors⁶⁴.

During the normal aging process, large amounts of myelin debris are generated, and microglia are responsible for phagocytosing and disposing the CNS of them. However, this process may become increasingly impaired during aging, leading to the accumulation of insoluble aggregates within microglia⁶⁵. Unable to dispose of their phagocytic cargo, microglia become dysfunctional and this impairment at the lysosomal processing level, seems to indicate that pathways downstream the engulfment stage are pivotal to proper microglial phagocytosis and overall CNS homeostasis.

Microglial phagocytosis has also been studied in the context of neurological pathologies like acute injury (e.g., stroke)^{26,66} and neurodegenerative diseases (e.g., Parkinson, Alzheimer)⁶⁶⁻⁶⁸. Some phagocytosis-related receptors have been implicated in the clearance of protein aggregates of A β and α -synuclein⁶⁹⁻⁷². Clearance of myelin debris, in studies conducted with multiple sclerosis models, has been reported to occur via MerTK, and TREM2 receptors (among others)⁷³. In the case of stroke, microglia are reported to have an active role in neuronal debris clearance. Furthermore, it is thought that overactive phagocytic microglia might phagocytose stressed but viable neurons through detection of transiently exposed PtdSer^{55,58}. This is thought to be one of reasons for the occurrence of post-stroke related neuronal injuries²⁶.

In conclusion, microglial clearance of debris, dead cells or protein aggregates is a crucial process for the maintenance of brain homeostasis and, as such, must exist in an optimal balance and be tightly controlled. Most of the research conducted on the topic of microglial phagocytosis is geared towards the Recognition stage. The following

stages – Engulfment, Trafficking/Maturation and Degradation – are assumed to be similar, if not equal, to the molecular mechanisms studied in other macrophages, since they possess the necessary elements to execute them. One of these mechanisms characterized in macrophages for the clearance of apoptotic cells is the microtubule-associated protein 1A/1B-light chain 3 (LC3)-dependent phagocytosis (LAP) ⁷⁴. A recent study has found evidence of a LAP-type mechanism (LC3-associated endocytosis (LANDO)) displayed by microglia for A β clearance ⁷⁰.

Microtubule-associated protein 1A/1B-light chain 3 (LC3)-dependent phagocytosis (LAP)

LAP is a type of phagocytosis triggered by receptor's recognition (e.g., TLR, PtdSer receptors) of pathogens or dead cells, followed by their engulfment into a single-membrane phagosome. Afterwards, there is mobilization of autophagy-associated machinery in addition to ROS production for phagosomal maturation and cargo degradation. Despite sharing many key components, LAP and autophagy are distinct mechanisms ⁷⁴ as we can see depicted in *Figure 7*.

There are three key complexes that define LAP's molecular mechanisms: (1) phosphatidylinositol 3-kinase (PI3KC3) complex for phosphatidylinositol 3-phosphate (PIP3) generation, (2) lipidated-LC3 production machinery and (3) NADPH oxidase 2 (NOX2) complex for ROS production.

Upon LAP induction and after phagosome formation, the PI3KC3 complex translocates to the single-membrane phagosome. This complex is formed by several proteins, namely, Beclin-1, vacuolar protein sorting (VPS) 34, VPS15 (known players in autophagy), Rubicon and UV radiation resistance-associated gene (UVRAG). While associated with UVRAG, Rubicon inhibits autophagy and seems to be required for LAP activation ^{75,76}. The PI3KC3 complex stability seems to rely on VPS34, as its deletion resulted in the loss of Rubicon, Beclin-1 and UVRAG from the phagosomal membrane ⁷⁶. VPS34 main function is to produce PIP3 to be incorporated in the phagosomal membrane, while Rubicon is responsible for the activation and stabilization of NOX2 ^{76,77}. Both the production of PIP3 and ROS are necessary for the recruitment and subsequent production of lipidated-LC3 ⁷⁶.

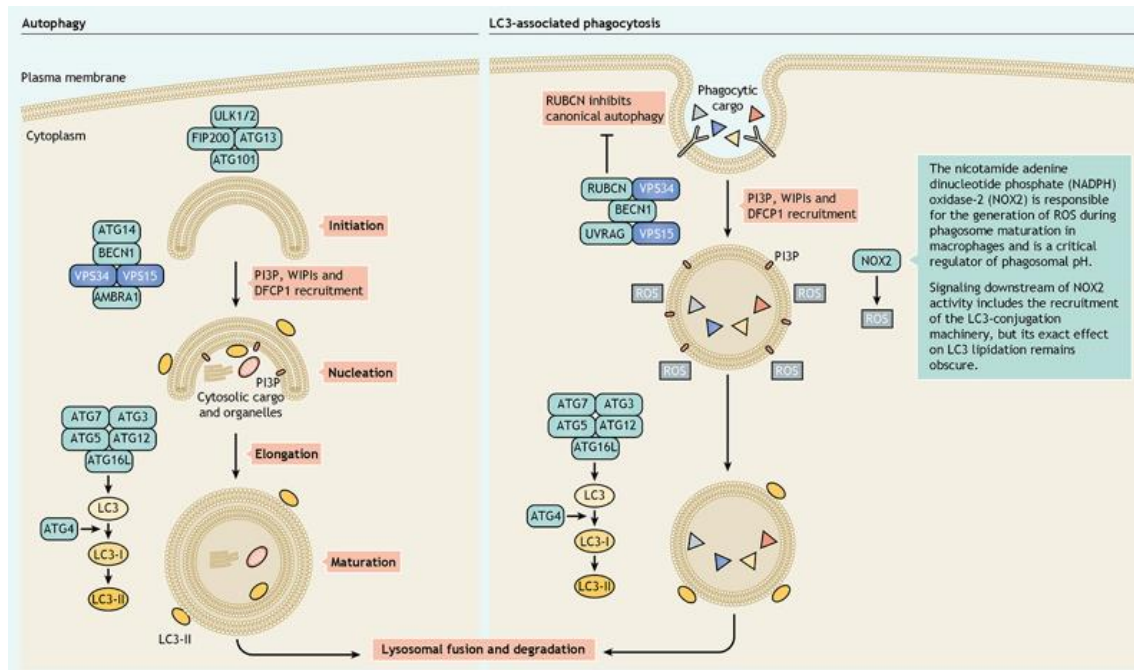


Figure 7 – LC3-associated phagocytosis in comparison with autophagy process. The image aims to showcase the differences between the canonical autophagy pathway and the non-canonical autophagy process known as LC3-associated phagocytosis (LAP). Despite sharing several key players, namely the production of lipidated LC3, both mechanisms differ in some key complexes. LAP does not require the initiation complex (ULK1/2, FIP200, ATG13 and ATG101) unlike autophagy that depends on it. They also differ in PI3K complex composition. Despite sharing three components (Beclin-1, VPS15 and VPS34), LAP additionally requires Rubicon and UVRAG, while autophagy needs ATG14 and AMBRA1. Finally, LAP requires NOX2 to promote phagosomal maturation and downstream signalling, while autophagy does not rely on it. Source: Heckmann and Green (2019) (doi: 10.1242/jcs.222984).

Mice deficient in Beclin-1, ATG5, ATG7 (required for autophagy and LAP), Rubicon and NOX2 (exclusively required for LAP) showed systemic lupus erythematosus like-syndrome, which was associated with the failed clearance of dying cells under homeostatic conditions. In addition, LAP-deficient (but not autophagy deficient) mice showed an increase in pro-inflammatory cytokine serum levels (e.g., IL-1 β , IL-6) and decreased anti-inflammatory cytokine IL-10 serum levels, after injection with UV-irradiated wild-type thymocytes⁷⁸.

Studies also indicate that Rubicon plays a role in phagosomal maturation progression and may act as a negative regulator of endocytic trafficking. Cells overexpressing Rubicon presented abnormal lysosomal morphology and reduced transport and degradation of endosomal cargo as well receptor recycling/degradation^{79,80}. Through genetic downregulation, it was shown that Beclin-1 reduced microglial engulfment of latex beads and A β . Beclin-1 deficiency prevented CD36 (recognizes the PtdSer “eat me” signal) and TREM2 receptor recycling, reducing microglial

phagocytic rate ⁶⁹. Similarly, the recycling of TREM2, CD36, and TLR4 was crippled in BV2 microglial cells deficient in ATG5 and Rubicon ⁷⁰.

Shahraz *et al.* conducted a study and observed that NOX2 knockout mice revealed decreased complement and phagocytosis-related pathways in comparison to control group, after LPS treatment. Furthermore, after repeated LPS application, NOX2 deficient animals showed reduced loss of dopaminergic neurons than their wild-type littermates ⁸¹.

Fundamental research provides intel and methodology that can offer support and ultimately translate into new clinical medicine applications. Researchers, in hopes of achieving such goal, have been searching for possible neuroprotective molecules that could be modulated in order to counteract injuries associated with neurodegenerative diseases and the aging process. The haem oxygenase (HO) system has been researched as a potential candidate for such applications ⁸²⁻⁸⁴.

1.4. Haem oxygenase and haem degradation products

Haem oxygenase (HO)

HO's is an enzyme whose main function is to degrade haem groups. In 1968, Tenhunen *et al* ⁸⁵ described that HO was able to degrade haem through the cleavage of the methylene bridge in the haemic ring, thus converting it into biliverdin (BV), in addition to releasing water, carbon monoxide (CO) and Fe²⁺ (*Figure 8*).

To this day, two catalytic isoforms of HO have been identified (HO-1 and HO-2). It was reported by McCoubrey *et al.* ⁸⁶ that a third isoform (HO-3) was present in the brain, thymus, prostate, testis, heart, kidney, liver and spleen of rats ⁸⁶. In addition, by isolating cDNA from rat brains, McCoubrey *et al.* were able to genetically characterize the three isoforms. Even so, HO-3 was deemed to be catalytically inactive, and its functions poorly understood.

According to the Human Atlas – Consensus dataset (<https://www.proteinatlas.org/ENSG00000100292-HMOX1/tissue>), HO-1 (32.8 kDa), also known as the inducible isoform, is generally expressed at low levels in most

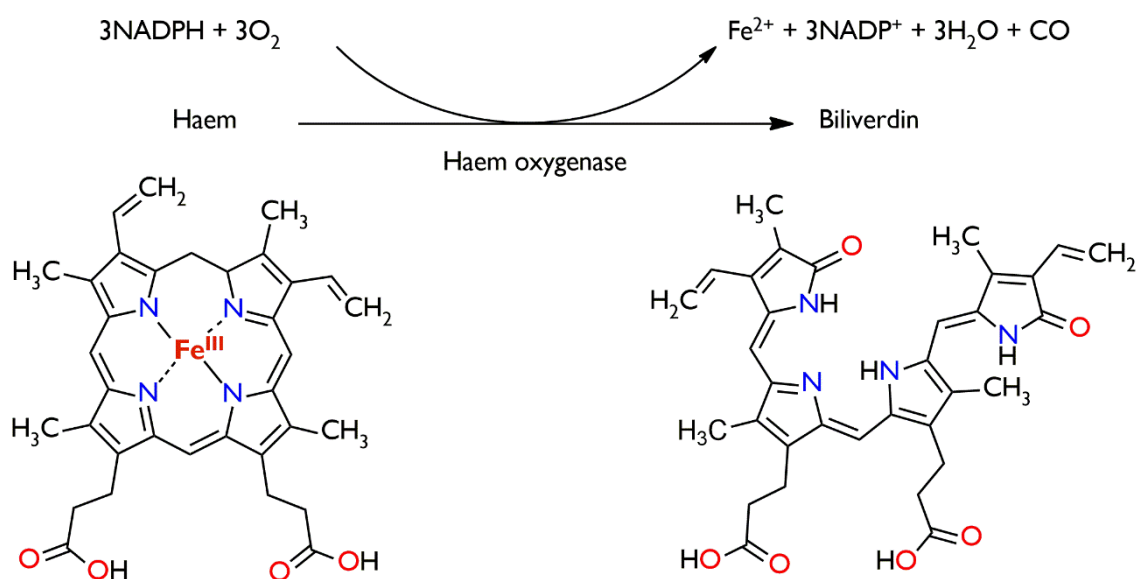


Figure 8 – Haem degradation reaction. Haem oxygenase, in the presence of NADPH and oxygen, degrades free haem into biliverdin, carbon monoxide, and ferrous iron. Adapted from: https://www.genome.jp/dbget-bin/www_bget?rn:R00311.

tissues, with the exception of the spleen. Despite its low levels, HO-1's expression can be induced in several tissues (e.g., the vasculature in the brain) in response to oxidative stress⁸⁶⁻⁸⁹, ultraviolet radiation^{90,91}, inflammation^{92,93}, hypoxia^{94,95}, heavy metals⁹⁶, hydrogen peroxide (H_2O_2)^{97,98} and NO^{99,100}. Studies have also shown that its expression naturally increases with age in both rat¹⁰¹ and human¹⁰² brains, and one may speculate it is due to aging-associated stresses.

Unlike its counterpart, HO-2 (36 kDa) is known as the constitutively expressed isoform. It is ubiquitously expressed, and is most prevalent in the heart muscle, testis, liver and brain (according to the Human Atlas – Consensus dataset (<https://www.proteinatlas.org/ENSG00000103415-HMOX2/tissue>)). HO-2's activity *in vivo* is rapidly increased without altering the enzyme's expression in response to both physiological and/or pathological stimuli, like glutamate, seizures, hypoxia, and hypotension¹⁰³. So far, HO-2's expression levels have shown a refractory response to the triggers that affect HO-1's transcription rate^{100,104}. However, adrenal glucocorticoids have been shown to influence HO-2's expression, due to a glucocorticoid responsive element in its genetic sequence, which is absent in HO-1^{105,106}. Table 2 comprises a summary of the molecular and biochemical features of these isoforms discussed throughout this section.

Table 2 – Catalytic haem oxygenase isoforms. Two haem oxygenase isoforms have been documented to have catalytic activity so far. This tables summarizes their main characteristics described throughout section 1.4.

	HO-1	HO-2
Main function	Haem degradation	Haem degradation
Inducibility	Inducible	Constitutive
Expression triggers	UV light [90,91] Inflammation [92,93] Hypoxia [94,95] Heavy metals [96] H ₂ O ₂ [97,98] NO [99,100]	Adrenal glucocorticoids [105,106]
Size (kDa)	32.8 (human) 33 (rat) 33 (mice)	36 (human) 35.8 (rat) 35.8 (mice)
Distribution (In humans)	Present in most tissues. Highly expressed in spleen.	Ubiquitously expressed. At higher levels in brain, testes, heart and liver.
Distribution (In rats ¹²⁹)	Present in most tissues Highly expressed in spleen and testes.	Present in most tissues Highly expressed in testes and thymus.
Distribution (In mice ¹³⁰)	Present in most tissues Highly expressed in spleen and liver.	Present in most tissues Highly expressed in testes.

Haem degradation and its reaction products are involved in physiological and pathophysiological processes that modulate cells' response to inflammatory, stress-inducing and apoptosis-triggering events ¹⁰⁷⁻¹¹¹. The cytoprotective aspects attributed to HO activity has been extensively studied and reviewed in the literature ^{82,112-117}. A by-product of haem degradation is free iron. Iron is a necessary cofactor for normal CNS functioning. Still, excessive amounts of iron within the brain can cause substantial oxidative damage to neuronal and glial cells. These injuries can in turn lead to neurodegeneration and neurologic dysfunction ¹¹⁸. Ferritin is a major iron storage

protein and by capturing Fe^{2+} can limit the risk it poses of provoking oxidative damage¹¹⁹. In addition, this release of iron through haem degradation has been shown to promote the induction of ferritin synthesis¹²⁰. This induction acts as a countermeasure to haem degradation-associated iron release, thus promoting cytoprotection.

Haem breakdown also generates BV, which is reduced to bilirubin (BR) by biliverdin reductase. There is evidence that suggest that BR has antioxidant properties. However, whether or not, physiological levels of bilirubin actually exert those antioxidant properties in a significant way remains controversial. The first hints of such properties came from the *in vitro* work done by Stoker *et al.*¹²¹ where they observed BR's antioxidant capacity surpassed that of α -tocopherol, a known potent antioxidant agent. Later experiments provided further evidence of such antioxidant potential in HeLa cells¹²², in rat primary cultures of cortical and hippocampal neurons¹²³ and in hyperbilirubinemic rats¹²⁴. Low concentrations of BR seemed to protect cells from 10,000-fold higher amounts of H_2O_2 . It was deduced from these observations that BR, once oxidized into BV, would be recycle back to BR through BV reductase's activity, thus allowing it to amplify its antioxidant effect. In addition, several epidemiological studies observed that above average serum bilirubin correlated with lower risk of ischaemic stroke and coronary artery disease^{125,126}. However, other studies put into question the physiological relevancy of BR's antioxidant capabilities^{127,128}.

Lastly, carbon monoxide is also a reaction product of haem oxygenase activity. HO activity generates one equivalent of CO per haem group degraded. This molecule is mostly known for its toxic properties. In spite of this, CO is an important signalling molecule and, when in the right concentrations (endogenous levels), can exert beneficial effects and help carry out several biological functions. This facet of CO will be explored in the following section.

1.5. Carbon Monoxide

CO is an odourless, colourless and flammable gas. It is one of the most abundant and widely distributed air pollutants, where the vast majority of its

emissions come from motorized vehicles ¹³¹. Its toxicity is mostly associated with its anthropogenic sources. CO poisoning may occur in situations of acute exposure to this gas due to its higher affinity to haemoglobin than oxygen ^{132,133}, reducing the amount of oxygen that is delivered and, consequently, utilized by tissues, promoting a hypoxic state. One must also consider other cytotoxic effects exerted by overexposure to CO, namely, the binding to other haem proteins (e.g., myoglobin and cytochrome c oxidase (COX)) that may alter their activity and signalling pathways ^{134,135}.

In spite of this, endogenous CO is mostly produced through the degradation of haem cofactors and can trigger several signalling pathways as well as carry out important biological functions. Studies often report that sub-lethal exogenous doses of CO can modulate these pathways in a cytoprotective way, often promoting anti-inflammatory, anti-apoptotic, vasodilatory, angiogenic and bactericidal effects, as well as modulate cell metabolism and cellular differentiation ^{136,137}. In summary, in the right concentrations, CO can produce diverse beneficial effects without being toxic to the organism.

1.5.1. Molecular targets underlying CO's biological functions

CO seems to exert its effects through its ability to interact with transition metals ¹³⁸ like nickel ¹³⁹, cobalt ¹⁴⁰, copper ¹⁴¹ and iron, which can be found within numerous haem- and non-haem proteins, thus influencing their activity in their respective signalling pathways. Soluble guanylate cyclase (sGC) is a ferric haem protein, mainly regulated by NO, but, to a lower extent, can be modulated by CO ¹⁴². With its ability to modulate sGC activity, CO is able to influence vasodilation ¹⁴³, neurotransmission ¹⁴⁴ and cell proliferation ¹⁴⁵. Several other important agents in prominent signalling pathways have been reported to be modulated by CO like mitogen-activated protein kinases (MAPK) ¹⁴⁶⁻¹⁵⁰, which can influence the expression of inflammatory cytokines like TNF- α , IL-1 β and IL-6 and increase anti-inflammatory ones like IL-10 ^{146,151}. In addition, there are reports that CO promotes the expression of factors like hypoxia-inducible factor-1 α (HIF-1 α) ¹⁵² and peroxisome proliferator-activated receptor γ (PPAR γ) ¹⁵³, as well as inhibit respiratory chain complexes and NADPH oxidase (NOX) ¹⁴⁹. CO has also been shown to influence certain transcription

factors like nuclear factor- κ B (NF- κ B), mitochondrial transcription factor A (TFAM) and nuclear respiratory factor (NRF) 1 and 2^{154,155}. Finally, low levels of CO also interact with COX, improving mitochondrial metabolism, which in turn prevents cell death¹⁵⁶ and promotes neuronal differentiation¹⁵⁷.

Studies have demonstrated that CO is able to either interact directly¹⁵⁸ or indirectly influence¹⁵⁹⁻¹⁶¹ K⁺, Ca²⁺ and Na⁺ ion channels, thus modulating signalling pathways dependent on the activity of these channels. Additionally, it has been reported that CO administration exerts bactericidal effects with little to no lethality to RAW 264.7 macrophages¹⁶².

1.5.2. Therapeutical potential of CO and the use of CO-releasing molecules

Knowing the beneficial effects of exogenous application of CO on experimental models, it is interesting to consider using CO for clinical purposes. However, it is complex to control the amount and organ specificity, when administering CO. Thus, researchers have invested in the creation of CO-releasing molecules (CORMs). CORMs are small chemical compounds specifically designed to release controlled amounts of CO. CORMs possess advantages over the classical CO delivery methods (e.g., inhalation), namely better dosage control. Depending on the molecule's chemical structure, CORMs present a plethora of options in regard to rate and amount of CO delivered over time. In addition, through careful ligand selection, tissue and/or organ specificity may be achievable^{163,164}. Furthermore, because CORMs allow for a more controlled dosage of CO, the risk of CO intoxication is significantly reduced. CO release, depending on the molecules structure, can be triggered in several different ways. The release is often triggered by reaching certain temperatures, enzyme activation, ROS activation, ligand exchange/substitution, pH change or exposure to light¹⁶⁵.

Nevertheless, these compounds still possess some limitations in terms of managing availability, solubility and stability of the CORM (i.e., some CORMs are relatively insoluble in water, or unstable in aerobic conditions). In addition, controlling CO release kinetics to a specific level is still a difficult task. It is thought

that the rate of CO release – whether it be in a fast burst or smaller doses over time – may determine the biological effect produced by the molecule. The majority of CORMs developed to this day are designed around a central metal ion (typically a transition metal such as iron, manganese or ruthenium). Pure organic CORMs have also been developed ^{166–168}. However, the majority are much less efficient than their inorganic counterparts in terms of CO release under physiological conditions. Due to the toxicity of transition metals, research in this field is shifting towards the construction of CORMs scaffolds with more biocompatible elements. *Table 3* depicts the molecular structure and physicochemical features of some of the CORMs developed so far ^{169–174}, while *Table 4* describes some studies (CO delivery method and pertinent results) conducted on CO's cytoprotective effects, detailed in the beginning of section 1.5.

Table 3 – CORMs. This table illustrates and describes physicochemical characteristics of several examples of CORMs, namely half-life and solubility under physiological conditions.

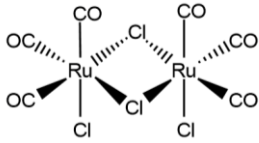
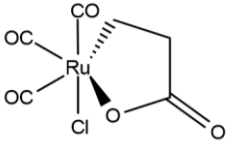
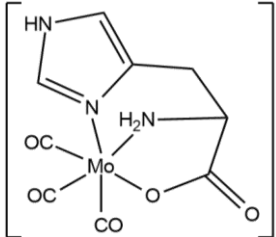
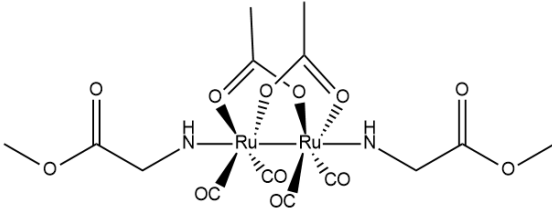
<p>[Ru(CO)₃Cl₂]₂</p>  <p>CORM-2</p> <p>$T_{1/2} \cong 1$ min Soluble in DMSO CO release: Ligand substitution</p>	<p>[Ru(CO)₃Cl-glycinate]</p>  <p>CORM-3</p> <p>$T_{1/2} \cong 1$ min Water Soluble CO release: Thermal degradation and ligand substitution</p>	<p>[NaMo(CO)₃(histidinate)]</p>  <p>ALF186</p> <p>$T_{1/2} = 25$ min Soluble in DMSO CO release: Ligand substitution</p>
<p>-----</p> <p>[(CH₃OCOCH₂NH)₂(Ru(CO)₂OCOCH₃)₂]</p>  <p>PhotoCORM</p> <p>$T_{1/2} \cong 7 - 12$ min Water Soluble CO release: Irradiation (360 nm)</p>		

Table 3 (cont.) – CORMs. This table illustrates and describes physicochemical characteristics of several examples of CORMs, namely half-life and solubility under physiological conditions.

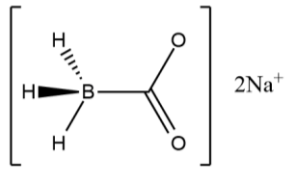
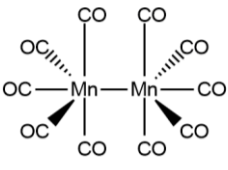
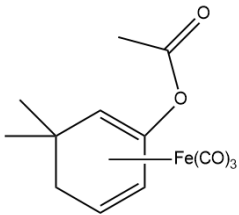
$[\text{Na}_2\text{H}_3\text{BCO}_2]$	$[\text{Mn}_2(\text{CO})_{10}]$	$[(\text{CH}_3)_2\text{C}_6\text{H}_5\text{OCOCH}_3](\text{Fe}(\text{CO})_3)$
		
CORM-A1	CORM-1	ET-CORM
$T_{1/2} = 21.06 \text{ min}$ Water soluble CO release: pH-dependent	$T_{1/2} < 1 \text{ min}$ Soluble in DMSO CO release: Exposure to light	$T_{1/2} \cong 133 \text{ min}$ Water Soluble CO release: Enzyme-triggered

Table 4 – Effects associated with CO application. This table serves as a summary of reported effects of CO application. CO delivery method and amount along with the results obtain for each study are described.

Effect	CO delivery	Result(s)	Ref.
Bactericidal	CORM-2 (25, 100, 150 and 200 mg/L)	Decreased <i>H. pylori</i> survival rate. Impairs the urease activity	[175]
	CORM-3 (25, 50, 75 or 100 μM)	Decreased <i>S. Typhimurium</i> survival rate.	[162]
Vasodilatory	CORM-3 (25, 50, 100 μM)	Promoted vasodilation of pre-contracted aortic rings in a concentration-dependent manner, through modulation of cGMP and potassium channels.	[143]
Vasodilatory and angiogenic	CORM-401 (10, 25, 50, 100 μM)	Vasodilation of pre-contracted aortic rings and angiogenesis processes were significantly enhanced. Induced angiogenesis via induction of HO-1 and phosphorylation of p38 MAP kinase.	[183]
Angiogenic	CORM-2 (100 μM)	CO promoted an increase of HIF-1 α protein levels, leading to increased VEGF protein production.	[152]

Table 4 (cont.) - Effects associated with CO application. This table serves as a summary of reported effects of CO application. CO delivery method and amount along with the results obtain for each study are described.

Effect	CO delivery	Result(s)	Ref.
Anti-apoptotic	CORM-2 (10, 50, 100 μ M)	Reduced cell apoptosis through NF- κ B signalling pathways	[154]
	CORM-2 (5 mg/kg)	Improved rat's mitochondrial and brain function. Increased PGC-1 α , NRF1, NRF2 and TFAM mRNA and protein expression	[155]
	CO gas (250 ppm)	Administration of CO prevented neuronal cell death through modulation of sGC, NO synthase and mitoK _{ATP} .	[176]
	ALF186 (10, 50, 100 mmol/L)	Attenuated cell apoptosis. CO influenced several haem-containing proteins (e.g., NOX, NO-synthase, sGC)	[177]
	CO gas (250 and 10,000 ppm)	Diminished apoptosis rate in endothelial cells. CO enhanced p38 MAPK activation.	[147]
Metabolic improvement	PBS saturated with CO (10 μ M or 50 μ M)	Increased COX specific activity and stimulated mitochondrial biogenesis. Enhanced Bcl-2 expression. By silencing Bcl-2 expression, CO metabolic effects were prevented.	[156]
Neuron differentiation	CORM-A1 (25 μ M)	Neuronal differentiation promoted by CO depended on the increase of reduced glutathione levels via metabolic regulation of pentose phosphate pathway. CO also promoted NADPH production.	[178]
	CORM-A1 (25 μ M)	Increased number of differentiated neurons through promotion of cell survival (increase in Bcl-2 expression, decrease in caspase-3 activity).	[179]

Table 4 (cont.) - Effects associated with CO application. This table serves as a summary of reported effects of CO application. CO delivery method and amount along with the result obtain for each study are described

Effect	CO delivery	Result(s)	Ref.
Anti-inflammatory	CORM-3 (10, 20, 30, 50 μ M)	CO induced HO-1 expression. HO-1 upregulation reduced IL-1 β -induced cell migration through inhibition of MMP-9 expression.	[180]
	CORM-2 (50, 100, 150 μ M)	Downregulated MMP-7 expression and inhibited the production of IL-6. Inhibited NF- κ B, AP-1 and C/EBP. Inhibited the expression of TNF- α , IL-1 β , MIP-1 β .	[181]
	CO gas (250 ppm)	Increased the expression of IL-10. ERK1/2 and JNK activation was unaffected. p38 MAPK activity was significantly increased as well as upstream kinases MKK3 and MKK6.	[146]
	CO gas (50, 250, or 500 ppm)	CO provided protection in a murine model of sepsis. Decreased IL-6 and IL-1 β . CO reduced JNK phosphorylation in murine macrophages and lung endothelial cells.	[150]
	CORM-2 (10, 20, 40 μ M) CO gas (250 ppm)	Increased the transcription of pyrin and increased the levels of IL-10. Reduced IL-1 β levels.	[151]
	CO gas (250 ppm)	CO upregulated expression of PPAR γ by provoking a burst in mitochondrial ROS production	[153]
Antioxidant	CORM-A1 (50 μ M)	Reduced ROS production by glutamate or the glutamate receptor agonist NMDA, AMPA and kainite	[182]

As demonstrated, CO possesses several distinct biological functions in a large variety of tissues, including the CNS. By acting on neurons, astrocytes and brain endothelial cells, CO participates in the promotion of CNS homeostasis and

cytoprotection. In the next section, we will explore how CO has been shown to modulate neuroinflammation and how it can regulate microglial function.

1.6. The role of carbon monoxide in mediating microglial immune response

As we have seen thus far, CO is able to generate a large variety of cytoprotective effects. In the case of modulating microglial immune response towards inflammatory stimuli, CO has been shown to influence inflammatory markers production/release, exert metabolic changes and modulate phagocytic activity¹⁸⁴ (Figure 9).

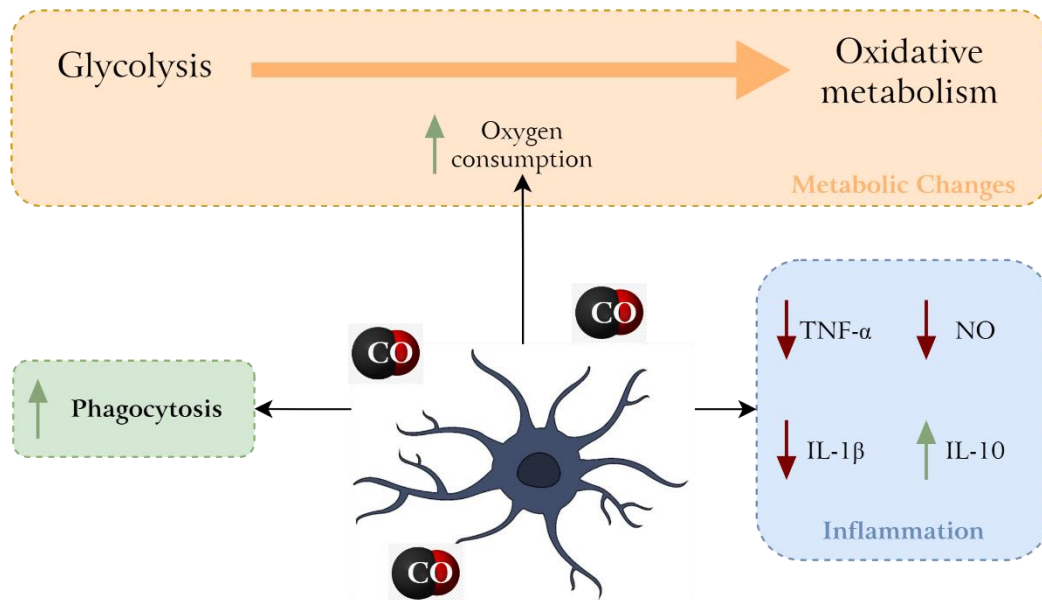


Figure 9 – Carbon monoxide’s effect on microglial function. CO has been shown to modulate several aspects of microglial function, when under an inflammatory stimulus, namely, metabolism, production and/or release of inflammatory and/or anti-inflammatory factors, as well as enhance phagocytic activity.

Application of CORM-3 molecule significantly reduced the inflammatory response (NO and TNF- α levels) of BV2 microglia, upon stimulation with thrombin, interferon- γ (IFN- γ) and hypoxia¹⁸⁵. In this study, they showed that this effect was independent of endogenous HO activity. Other studies have also observed similar changes^{186,187}. CO promoted the decrease in nitric oxide synthase (iNOS) expression, thus prompting a decrease in NO. Administration of CO also led to the increase in IL-10 release¹⁸⁷.

CO also induced metabolic changes in microglia cells. BV2 cells, after exposed to inflammatory stimuli such as LPS, decreased their oxidative phosphorylation rate and increased their glycolytic rate. At low concentrations, CO has been shown to increase microglia's oxygen consumption, thus promoting a shift back towards oxidative phosphorylation^{186,187}.

Regarding microglial phagocytosis, treating microglial cells with CO has been shown to influence microglial phagocytic capacity. The stimulation of HO-1 led to a reduction in microglial migration as well as a decrease in apoptotic neuron engulfment¹⁸⁸.

Mice with HO-1-deficient microglia showed impaired erythrophagocytosis along with higher amounts of neuronal injuries and levels of cognitive dysfunction. These effects were rescued by administration of CO via inhalation¹⁸⁹. Another study corroborated the importance of proper function HO-1 during erythrophagocytosis¹⁹⁰. However, they present different results in terms of exogenous CO effect on erythrophagocytosis without proper HO-1 function. Kaiser *et al.*¹⁹⁰ also showed that CO led to the reduction of CD36 surface expression, a receptor which was proven to be extremely important for erythrocyte clearance.

In summary, as we've seen throughout sections 1.5 and 1.6, CO exerts effects on a wide range of proteins and manages to influence a plethora of different pathways, namely ones involved in immune response regulation, apoptosis prevention and the phagocytic process. In the context of microglial phagocytosis, the molecular mechanisms behind it are still poorly understood, especially the ones pertaining to the engulfment, trafficking and cargo degradation stages of the process. It is often assumed that microglial phagocytic process is similar, if not equal, to other macrophages because they possess most, if not all, the necessary machinery to execute the molecular mechanisms described in other macrophages. Overall, administration of CO seems to influence microglia and other macrophage's immune response, generally by facilitating the phagocytic process, through promotion of receptor recycling^{190,191}, proper phagosomal maturation¹⁹² and attenuation of the pro-inflammatory state¹⁸⁵⁻¹⁸⁷, shifting it towards a more anti-inflammatory one.

1.7. Final remarks and objectives

Phagocytosis is a crucial mechanism through which microglia execute a plethora of essential biological functions. Through phagocytosis, microglia are able to manage synaptic pruning and the clearance of dead cells, pathogens, protein aggregates and cellular debris, which are all key steps towards maintaining homeostasis within the CNS.

CO has been shown to possess several cytoprotective traits, namely increasing neuron survival in hypoxic conditions by promoting a more anti-inflammatory phenotype in microglia. Preliminary data obtained in our lab by Dr. Nuno Soares has shown that CO can enhance microglial engulfment of dead neurons, while sparing viable ones. However, there is still much left unknown in term of how CO operates to promote this effect on the phagocytic process.

Thus, the main goal of this thesis is to explore CO's modulation of microglial phagocytosis of dead/dying neurons. This work will explore CO's impact on three of the four stages of phagocytic events – target engulfment, phagosomal trafficking and cargo degradation. In addition, the novel molybdenum-based CORM ALF826 is used to explore CO's effects in the context of microglial phagocytosis. ALF826 is a molybdenum-based CORM developed by Dr. Carlos Romão from ITQB/Proterris. CORMs designed around a molybdenum-based centre are a mark of progress in overcoming the toxicity risk transition metals in CORMs pose. Molybdenum is a biocompatible transition metal, because it already plays an essential biological role in the organism¹⁹³. Furthermore, metabolic studies have shown that, after intravenously or dietary intake of molybdenum, there is a rapid clearance of excess of this metal¹⁹⁴. This metabolic adaptation towards promoting molybdenum turnover, upon increased intakes, serves as a protection against possible toxic effects molybdenum might cause.

This thesis will provide a deeper look into the lysosomal function aspect of phagocytosis resolution (*Figure 10*). While assessing each stage, we intend to answer three main questions:

(1) Does CO exhibit inhibit or facilitate cargo engulfment by microglia (in the presence and absence of LPS-induced inflammation)?

- (2) Does CO prevent or facilitate phagosomal trafficking into lysosomes?
- (3) Does CO promote or inhibit degradation of phagosomal cargo by interfering with lysosomal activity?

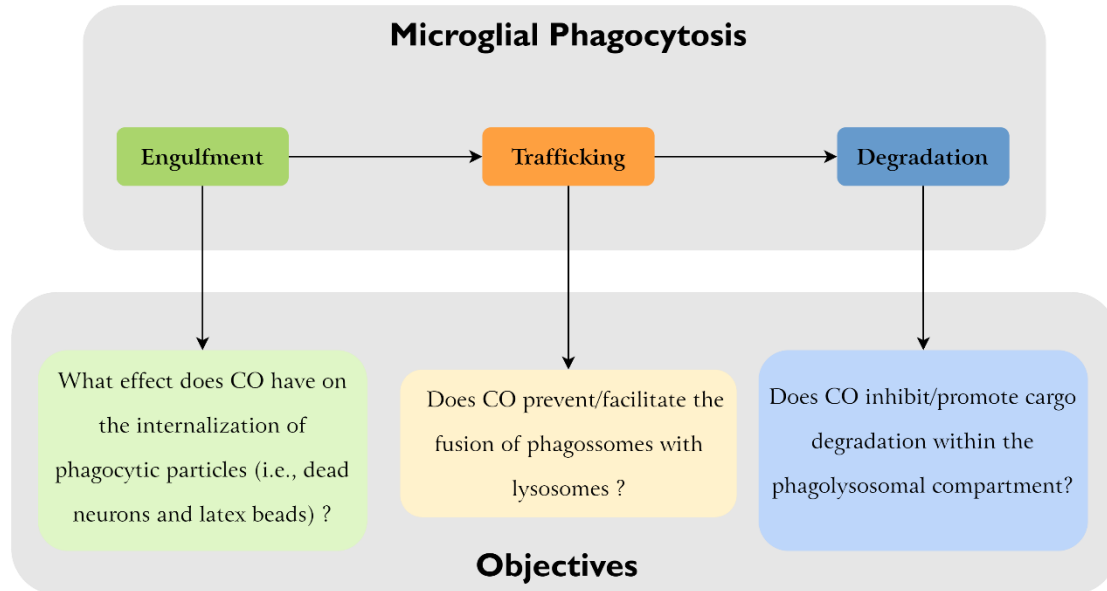


Figure 10 – Main questions aimed to answer in this thesis.

The insight provided by this work will not only help elucidate how CO might affect microglial phagocytosis, both in the presence and absence of inflammatory stimuli, but also shed light on its impact on the lysosomal function and the repercussions it has on microglial phagocytic rate.

Chapter 2

Materials and methods

Chapter 2 - Materials and methods

2.1. Cell cultures

2.1.1. BV2 cell line

BV2 murine microglial cells were cultured in RPMI-1640 (*Sigma-Aldrich*) medium supplemented with 10% of inactivated Fetal bovine serum (FBS) (*Thermo-Fisher Scientific*), penicillin (100 units/mL) and streptomycin (100 $\mu\text{g}/\text{mL}$) (*Thermo-Fisher Scientific*) and 4 mM of L-glutamine (*Thermo-Fisher Scientific*) in cell culture flasks and kept at 37 °C and 5 % CO₂ in a humidified incubator.

2.1.2. CAD cell line

CAD murine neuron cells were cultured in Dulbecco's Modified Eagle Medium/F12 (DMEM/F12) (*Thermo-Fisher Scientific*) medium supplemented with 10% of inactivated FBS, penicillin (100 units/mL) and streptomycin (100 $\mu\text{g}/\text{mL}$) and 4 mM of L-glutamine in cell culture flasks and kept at 37 °C and 5% CO₂.

2.2. ALF826 preparation

ALF826 was provided by Proterris (Portugal) Lda. Stock solutions of 2.5 mM were prepared by dissolving the compound in dimethyl sulfoxide (DMSO, *Sigma-Aldrich*) and diluting it 1/10 in a NaHCO₃ solution (0.1mM, pH 8.3). ALF826 was then filtered, aliquoted and stored at -80°C at a final concentration of 2.5 mM.

2.3. Bead engulfment assays

In order to optimize the protocol for the assessment of bead engulfment rates and to determine the optimal engulfment conditions, two different protocols were tested: A and B, as described below:

Protocols:

A.

24 multi-well (MW) plates with glass coverslips were used to plate, approximately, 6×10^4 BV2 cells in each well. The cells were plated in 1 mL of BV2 culture medium with 10% non-inactivated FBS.

For this protocol, it was necessary to opsonize the beads. 20 μL or 35 μL of 10% (m/v) bead solution (*Sigma Aldrich*, LB30, 3 μm) were washed with phosphate buffered saline (PBS) and spined-down thrice. Afterwards, PBS was removed, and the beads were incubated with 1.7 $\mu\text{g}/\mu\text{L}$ human IgG overnight at 4 °C, under slow rotation. The next day, beads were once again washed with PBS and spined-down thrice. The medium in which the cells were cultured was replaced with 150 μL of FBS-free culture medium. Next, 6.5 μL of beads were added, making the final concentration per well 1.3% or 2.3% (m/v). After adding the beads, cells were incubated at 37 °C and 5 % CO₂ for 5, 10, 20 or 30 min.

Immunofluorescence.

Upon completing the established timepoints, medium was removed, and cells were washed twice with PBS, followed by fixation with 4% v/v paraformaldehyde (PFA) (with 4% w/v sucrose) solution. Coverslips were washed thrice with PBS and blocked with 0.1% bovine serum albumin (BSA, *Merck*) and 0.1% Triton X-100 in PBS for 30 min at room temperature. Next, cells were incubated with Cy5 (*Jackson ImmunoResearch*, AB_2340539, 1:500) for 1 h at room temperature, in order to distinguish between engulfed and non-engulfed beads. Afterwards, they were washed thrice with PBS and cells were permeabilized with 0.3% Triton X-100 in PBS for 15

min at room temperature. Coverslips were once again blocked with 0.1% BSA and 0.1% Triton X-100 in PBS for 30 min at room temperature after being washed thrice with PBS. Cells were then incubated with phalloidin-Alexa Fluor (AF) 555 (*Invitrogen*, A30106, 1:400) to stain microglia. Finally, the coverslips were washed thrice with PBS and mounted on microscope slides with ProLong Gold antifade Mountant (*Invitrogen*, P36935) and stored at 4 °C.

Fluorescence microscopy.

Samples were observed under a confocal microscope (*Zeiss*, LSM710). Using ZEN software, three random images of each condition combination (timepoint and bead concentration), viewed through a 63x objective, were collected. Microglia cells were stained with phalloidin-AF555 (orange/red). Non-engulfed beads were stained with Cy5 (red), while engulfed one were left unstained and were observable under transmitted light. All image analysis was performed using Fiji software (*ImageJ*).

B.

For B protocol, 1 μm fluorescent beads were used (*Sigma*, #L1030). 24 MW plates with glass coverslips were used to plate BV2 cells. Five assays (B1, B2, B3, B4 and B5) were conducted using this protocol with some variances among them (*Table 5*). Assays B1 and B2 were done to optimize the used bead concentration as well as the incubation time with microglia. The remaining assays (B3 – B5) were done to optimize and test CO's effect on the engulfment stage under inflammatory and non-inflammatory conditions. Cells were plated in 500 μL or 1 mL of culture medium with 2% or 10% inactivated FBS. The following day (24 h), some cells were treated with 50 μM of ALF826 (CO delivery method). After 24h hours, some wells were treated with 0.5 $\mu\text{g}/\text{mL}$ LPS to induce inflammation. The next day, the medium in which the cells were plated was replaced with 200 μL of BV2 culture medium with 2% or 10% inactivated FBS. Afterwards, 1, 2 or 4 μL of 0.025% bead solution was added to the wells, making the final concentration in the wells 0.00125%, 0.025% and 0.05%, respectively. Cells were then incubated with the beads at 37 °C and 5% CO₂ for 30, 60 or 70 min.

Table 5 – Assays conducted according to protocol B. This table describes the assays conducted according to protocol B and the variances between assays.

	B1	B2	B3	B4	B5 **
Seeding	6x10 ⁴	6x10 ⁴	8x10 ⁴	8x10 ⁴	8x10 ⁴
Well volume	500 μ L	500 μ L	500 μ L	1 mL	1 mL
FBS (%)	2%	2%	2%	2 or 10% *	10%
Well volume (before adding beads)	200 μ L	200 μ L	200 μ L	200 μ L	200 μ L
Timepoints (min)	30, 60 and 70	30 and 60	60	60	60
[Bead] (final concentration)	0.00125%, 0.025% and 0.05%	0.00125% and 0.025%	0.025%	0.025%	0.025%
LPS	No	No	0.5 μ g/mL	0.5 μ g/mL	0.5 μ g/mL
ALF826	No	No	50 μ M	50 μ M	50 μ M

* Some wells were plated with culture medium containing either 2% or 10% FBS.

** This assay was conducted with two biological N's. All other assays were performed using only one.

Immunofluorescence.

After the established timepoints, the medium was removed, cells were washed twice with PBS and fixed with 4% v/v PFA (with 4 % w/v sucrose) solution. Coverslips were again washed twice with PBS and cells were permeabilized with 0.3% Triton X-100 in PBS. Next, they were washed twice with PBS and blocked with 0.1% BSA and 0.1% Triton X-100 in PBS for 30 min at room temperature. Afterwards, cells were incubated with phalloidin-AF555 (*Invitrogen*, A30106, 1:400) for 1 h at room temperature. Finally, the coverslips were washed twice with PBS and mounted on microscope slides with mounting medium (*Invitrogen*, P36935) and stored at 4 °C.

Fluorescence microscopy.

Samples were observed under a widefield microscope (*Zeiss*, Axio Imager Z2). Using ZEN software, four to seven images, viewed through a 63x objective, of each condition combination (timepoint and bead concentration) were collected. Microglia

were stained with phalloidin-AF555 (red), and their nuclei were stained with DAPI (blue). Beads emitted green fluorescence. Using the microscopic images acquired during this protocol and through the application of *Equation A*, we were able to assess cell's phagocytic efficiency. Assays B1 and B2 served to optimize protocol B in order to better assess CO's effect on the engulfment stage, during assays B3, B4 and B5. All image analysis was performed using Fiji software (*ImageJ*).

$$\text{Phagocytic Efficiency} = \frac{(1 \times c_1 + 2 \times c_2 + \dots + c_n)}{\text{Total number of cells}}$$

Equation A – Phagocytic Efficiency. The variable c_n represents the number of cells that contain n beads ($n = 1, 2, 3, \dots$) up to a maximum of 10 points for 10 or more beads per cell.

2.4. DQ-BSA degradation assays

In order to assess how CO affects the degradative capability of lysosomes, we conducted several assays in which we assessed the degradation of DQ-BSA, which is a self-quenched fluorescent molecule. The general protocol is described in *Table 6*.

Table 6 – Degradative capacity protocol. This table broadly describes the protocol applied to study the degradative capacity of lysosomes in BV2 cells when treated with CO under inflammatory and non-inflammatory conditions.

	0 h	24 h	48 h	72 h
BV2	Plate (96 MW)	Treat with ALF826	Treat with LPS	(1) Remove medium
				(2) Wash with PBS
				(3) Add DMEM F12 (without phenol red)
				(4) Add DQ-BSA
				(5) Incubate for 3 h
				(6) Measure DQ-BSA fluorescence (645 nm) for 4 h every 10 min interval.

BV2 cells were plated in 96 MW black plates (1.54×10^4 cells per well) using BV2 culture medium with 10% FBS (200 μ L per well). 24 h later cells were treated with 50 μ M of ALF826 and after another 24 h period microglia were treated with 0.5

$\mu\text{g/mL}$ LPS. The following morning (24 h later), the medium was removed, cells were washed with PBS, and fresh DMEM/F12 medium (without phenol red) (*Gibco*, 11039-021) was added. 20 $\mu\text{g/mL}$ DQ-BSA (*Invitrogen*, D12051) was then added to the microglial cultures and left incubating for 3 h at 37 °C and 5% CO₂. After said time period, cells were washed once with PBS and the decrease of fluorescence was measured using (*BioTek*, Synergy HT), acquiring readings at 645 nm for 4 h every 10 min interval. During this 4 h the cells are kept at 37 °C.

2.5. Neuron engulfment assays

Firstly, we intended to find the optimal ratio (neuronal to microglial cells) and incubation period to determine the best conditions for engulfment assessment.

Using separate 24 MW plates, we plated CAD neurons (8×10^4 cells) and BV2 microglia (6×10^4 cells). CAD cells were plated in 1 mL CAD culture medium (previously described) and BV2 cells were plated in 1 mL of BV2 culture medium with 0.5% inactivated FBS. After a 48 h period, neurons were treated with 20 μM *tert*-butyl hydroperoxide (*t*-BHP) (*Sigma-Aldrich*) to induce neuronal death. The next day, after cell counting, neurons were stained with 5-(and-6)-carboxytetramethylrhodamine succinimidyl ester (TAMRA) (*Sigma-Aldrich*, 21955, 1:2000) for 15 min at 37 °C and 5% CO₂. Afterwards, neurons were collected from the wells into centrifuge tubes and centrifuged for 5 min at 1000 relative centrifugal force (rcf) and supernatant was eliminated. The pellet was resuspended in PBS and this process was repeated until excess TAMRA was removed (about 3 washes were needed). Upon finishing these washes with PBS, the pellet was resuspended in BV2 culture medium with 0.5% inactivated FBS. BV2 cells' medium was replaced with 0.5 mL of BV2 culture medium with 0.5% FBS, containing isolectin B-4 (IB4) coupled to AF488 (*Invitrogen*, I21411, 1:1000) in order to stain microglia. Apoptotic neurons, now resuspended in BV2 culture medium with 0.5% inactivated FBS, were added into microglial culture, according to the ratios of neuron to microglia defined beforehand for the optimization process (1:1 and 1:2). Both cell types were incubated together for pre-defined timepoints (1 h, 2 h, 3 h or 5 h) at 37 °C and 5 % CO₂.

Upon completing these timepoints, live cells were observed under an inverted microscope (*Zeiss, Axiovert 40 CFL*), using a 20x objective. Four to six images per condition combination were analysed by assessing the ratio of TAMRA-positive BV2 microglia to total BV2 cells (stained with AF488-tagged IB4). All image analysis was performed using Fiji software (*ImageJ*). While assessing CO's effects, the incubation period and ratio selected were 2 h and a 1:2 ratio.

Assessing CO's effects

The protocol was conducted accordingly to what is described in *Table 7* and followed what has been described before in addition to treating BV2 cells with CO and LPS. After plating BV2 cells, 24 h later, they were treated with 50 μ M of ALF826. The following 24 h, BV2 cells were treated with 0.5 μ g/mL LPS. 72h after plating both cultures, neurons were added to microglia in a 1:2 (neuron to microglia) ratio and left incubating for 2 h at 37 °C and 5% CO₂. Two techniques were used to evaluate the engulfment of dead neurons by microglia: live fluorescence microscopy (*Axiovert*) and flow cytometry (*Canto II*).

Table 7 – Protocol used to study neuronal debris phagocytosis. This table broadly describes the experimental setting used to study CAD neuronal debris phagocytosis by BV2 microglia, when treated with CO under inflammatory and non-inflammatory conditions.

	0 h	24 h	48 h	72 h
BV2	Plate (24 MW)	Treat with ALF826	Treat with LPS	(1) Count cells (2) Stain CAD with TAMRA (3) Centrifuge and collect neuronal debris (4) Replace medium and stain BV2 with AF488-tagged IB4
CAD	Plate (24 MW)	-	Treat with <i>t</i> -BHP	(5) Add neurons to microglia (6) Incubate cells (7) Analysis: Axiovert, Canto II, LSM710

2.5.1. Live imaging

In order to assess microglial phagocytosis of dying neurons and how CO and inflammation affects this process, live imaging was performed. Upon completing the 2 h incubation period, cells were observed under an inverted fluorescence microscope (*Zeiss, Axiovert 40 CFL*), using a 20x objective. For each assay, four to five images were obtained from each condition. Images were analysed by assessing the ratio of TAMRA-positive BV2 microglia to total BV2 cells (stained with AF488-tagged IB4). All image analysis was performed using Fiji software (*ImageJ*).

2.5.2. Flow cytometry

After the 2 h incubation period, co-culture of neurons and microglia cells were collected to test tubes and analysed through flow cytometry as soon as possible. FACS Canto II (BD Biosciences) cytometer was used to measure samples fluorescence through the AF488 (green) and PE (red) channels. 488nm laser line was used for excitation. To exclude CAD cells, non-engulfed debris and other events, AF488 negative events were gated out of the analysis. Microglia phagocytic rate was analysed by quantifying median PE fluorescence intensity of AF488 positive events (microglia). 10 000 events were analysed per condition at medium speed. Appropriate controls, such as positive staining controls and unstained samples were made, allowing for the adjustment of auto-fluorescence levels and compensation parameters. Post-acquisition data analysis was conducted with the FlowJo software (*BD Biosciences*).

2.6. Lysosomal-associated membrane protein-I localization assessment

With the intent of evaluating phagosomal cargo trafficking into lysosomes, we assessed the co-localization of the lysosomal-associated membrane protein-I (LAMP-1) with neuronal debris-containing phagosomal compartments via immunocytochemical experiments. The assays conducted to achieve this objective

followed the protocol described in *Table 7* (subsequent analysis was conducted through confocal microscopy (LSM710)).

Immunofluorescence.

After incubating microglia for 2 h at 37 °C and 5% CO₂, cells were washed with PBS twice and then fixed with 4 % PFA solution (with 4% sucrose) for 20 min at room temperature. Coverslips were then washed again with PBS and cells were permeabilized with 0.3% Triton X-100 in PBS for 15 min at room temperature. Afterwards, cells were once again washed and afterwards blocked with 0.1% BSA and 0.1% Triton X-100 in PBS for 30 min at room temperature. Incubation with anti-LAMP-1 antibodies (*Abcam*, ab24170 1:300) was conducted at room temperature for 2 h. After being washed twice with PBS, coverslips were incubated with AF647 antibodies (*Abcam*, ab150079, 1:400) for 1 h at room temperature. In the end, coverslips were mounted in microscope slides with mounting medium (*Invitrogen*, P36935) and stored at 4 °C.

Fluorescence microscopy.

Samples were analysed with a confocal microscope (*Zeiss*, LSM710). Using ZEN software, four to ten images were collected per condition, using a 63x objective. Microglia cells were stained with AF488-tagged IB4 (green), neurons and neuronal debris were stained with TAMRA (yellow/orange), and LAMP-1 protein was stained with AF647 (red). Data was analysed by evaluating the ratio of neuron debris-containing microglia and total number of microglia per image. All image analysis was performed using Fiji software (*ImageJ*).

2.7. Statistical Analysis

The data is presented throughout this work as mean \pm standard error of the mean (SEM). Data normalcy was tested through the Shapiro-Wilk normality test. Data that was found to follow a normal distribution was then assessed through an

ordinary one-way or two-way ANOVA test, followed by Tukey's multiple comparison test, considering a 95% confidence interval. On the other hand, data that did not follow a normal distribution was evaluated through the Kruskal-Wallis test, followed by Dunn's multiple comparison test, considering a 95% confidence interval as well. Statistical significance is represented by stars (*). P-values ≤ 0.05 are represented by one star, P-values ≤ 0.01 by two stars, P-values ≤ 0.001 by three stars and P-values ≤ 0.0001 by four stars. Non-significant p-values ($P \geq 0.05$) were omitted in graphical data representation. All statistical analysis was performed using the Prism 8.0.2 software (*GraphPad*).

Chapter 3

Results

Chapter 3 - Results

3.1. Engulfment stage

3.1.1. Phagocytosis protocol optimization: bead engulfment assays

Phagocytosis, in a simplistic way, can be viewed as a sequence of four stages – recognition, engulfment, trafficking/maturation and degradation of phagocytosed cargo. Our main goal is to explore CO's effects in the last three stages of this process. In order to do so, we started by determining the optimal conditions for target engulfment by BV2 microglia. Two different protocols (described in chapter 2) and type of beads were used.

To summarize, in protocol A, we added 3 μm IgG-opsonized latex beads to microglial cultures and assessed their engulfment. After for 5, 10, 20 or 30 min, microglia were fixed and stained with phalloidin-AF555 (orange). In order to distinguish between engulfed and non-engulfed bead, before permeabilization, beads were stained with Cy5 antibodies (red). This way, beads that were outside microglia's plasma membrane would be stained with a red colour and unstained beads are presumably internalized.

Following protocol A, we assessed bead engulfment using confocal microscopy. However, we observed that cells were not engulfing more than 1 or 2 beads, regardless of incubation time or number of beads supplied (*Figure 11*). Therefore, protocol A did not allow for the establishment of optimal engulfment conditions due to its low efficiency.

Considering that the previous protocol was not efficient enough to conduct a proper assessment of the engulfment stage, we decided to move on to a new protocol (protocol B). We conducted a series of assays (B1 – B5) according to the protocol B, described in chapter 2. In short, protocol B consisted in adding 1 μm fluorescent (green) latex beads to microglial cultures. The first assays (B1 and B2) served to optimize experimental variables (incubation time and bead concentration), while the

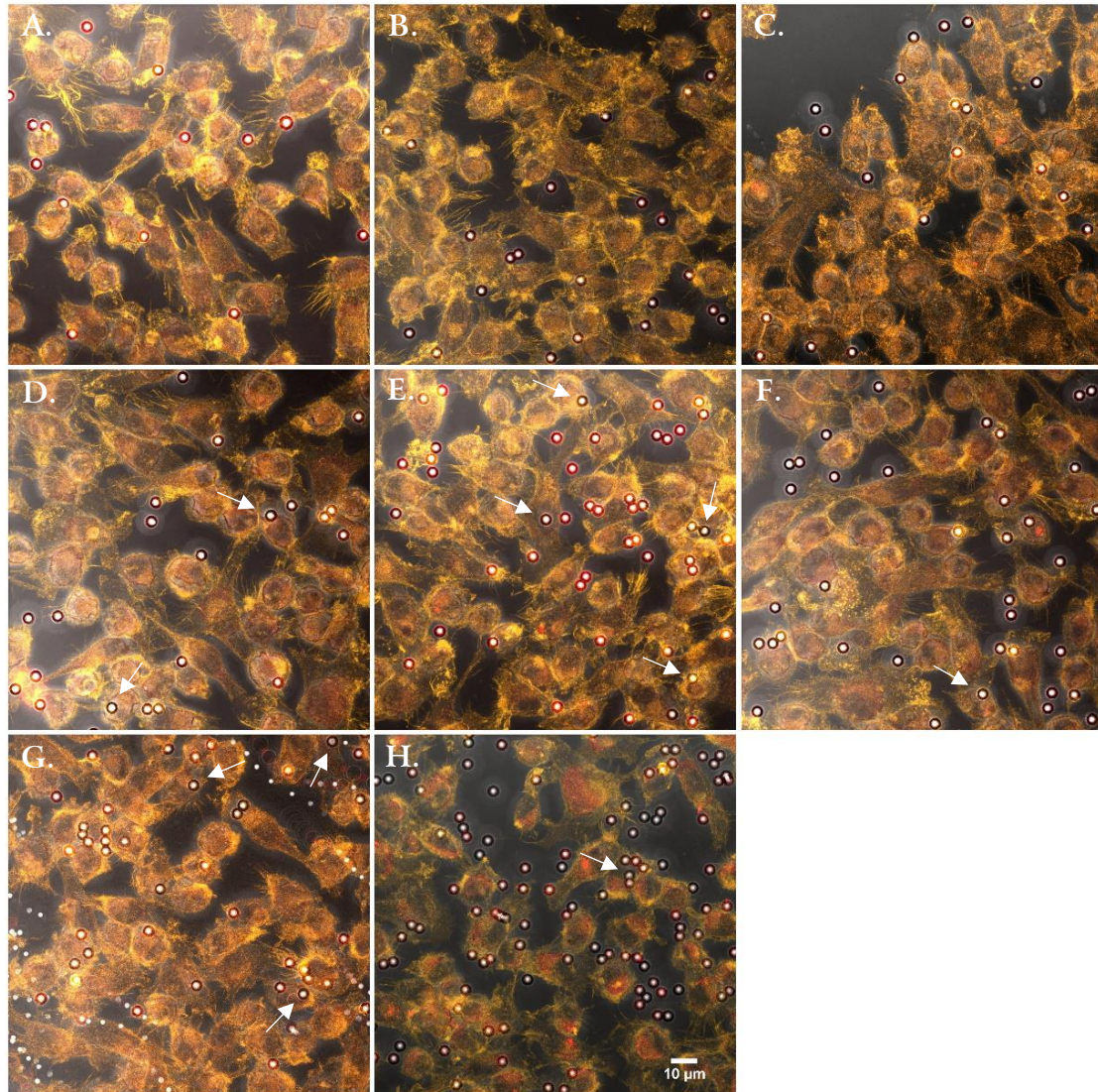


Figure 11 – Bead engulfment assay following protocol A (optimization). (A – B) Confocal images of cells that were incubated for 5 minutes, after adding 1.3% (A) or 2.3% (B) bead solution. (C – D) Confocal images of cells that were incubated for 10 minutes, after adding 1.3% (C) or 2.3% (D) bead solution. (E – F) Confocal images of cells that were incubated for 20 minutes, after adding 1.3% (E) or 2.3% (F) bead solution. (G – H) Confocal images of cells that were incubated for 30 minutes after adding 1.3% (G) or 2.3% (H) bead solution. Microglia was stained with phalloidin-AF555 antibodies (orange), and non-engulfed beads were tagged with anti-IgG antibodies (red). Arrows indicate engulfed beads.

other three (B3 – B5) were conducted in order to assess CO's effects in phagocytic efficiency. Unlike the previous two assays (B1 and B2), during assays B3 – B5, cells were treated with CO and LPS. Upon completing the incubation period, microglia were fixed and stained with phalloidin-AF555 (red), and their nuclei were stained with DAPI (blue). Phagocytic efficiency was assessed through the analysis of z-stack images obtained with the Z2 fluorescence microscope. Assay B3 served to optimize FBS concentrations (detailed in *Table 5* in chapter 2). Since 2% FBS concentration was too low and cells did not grow properly, assay B3 was discarded, and assays B4 and B5

were used (10% FBS). The results for assays B1 – B2 are displayed in *Figure 12*, while the results obtained from assays B4 – B5 are presented in *Figure 13*.

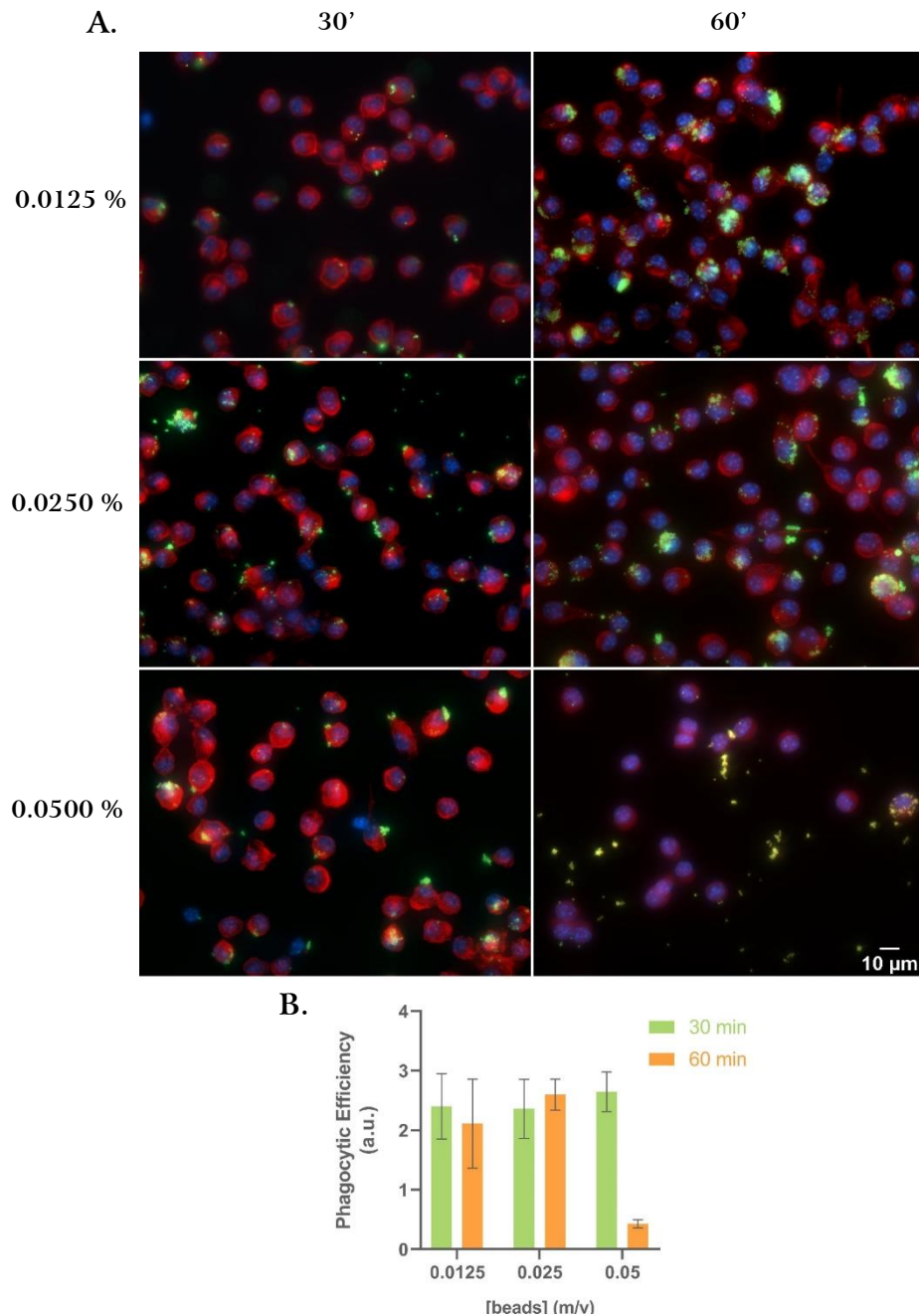
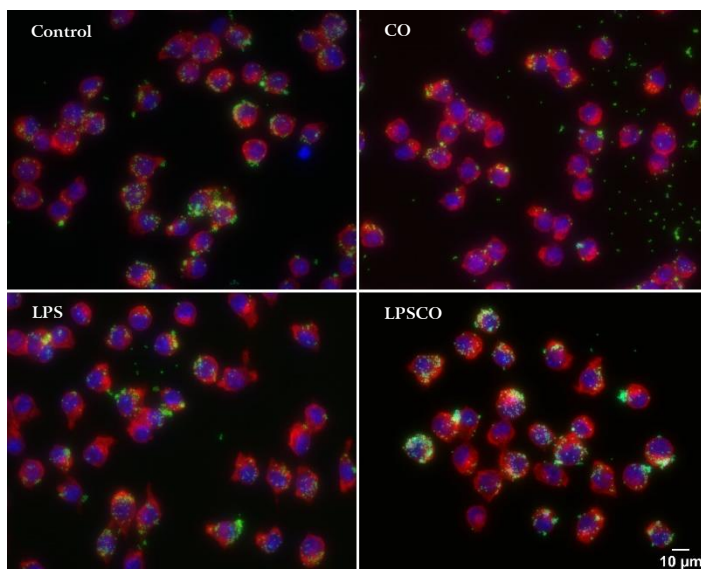


Figure 12 – Bead engulfment assays following protocol B (optimization). (A) Representative Z2 microscope images from the two assays (n=2) conducted (B1 and B2). Microglia is stained with phalloidin-AF555 (red) and incubated with fluorescent latex beads (green). Nuclei is stained with DAPI (blue). (B) Optimization of variables – bead concentration and incubation time – for protocol B. Bar graph depicts the average phagocytic efficiency obtained for each condition. Three to five images were analysed per condition, by applying Equation A (described in Chapter 2). An average of 149 cells were analysed per condition. Statistical significance between groups was calculated first through an ordinary two-way ANOVA test, followed by Tukey’s multiple comparison test. P-value significance is represented by stars (*). P-values ≤ 0.05 (*), ≤ 0.01 (**), ≤ 0.001 (***) and ≤ 0.0001 (****), while non-significant relationships were omitted. Error bars illustrate SEM.

During the optimization process (assays B1 and B2), due to the formation of bead clumps and low cell count in one of the assays, analysis of bead engulfment was compromised and may have led to the large variation observed in the bar graph (*Figure 12*). In spite of this, the results obtained led us to conclude that the conditions 60 min and 0.025 (m/v) bead solution were the optimal ones, as supported by the literature consulted¹⁹⁵.

In *Figure 13* and using protocol B, there is a significant increase in microglia phagocytic efficiency under inflammatory condition (LPS-treated groups). However, CO failed to produce any statistically significant alteration in phagocytic efficiency in both inflammatory and non-inflammatory conditions. Nevertheless, there is a tendency for CO to decrease LPS-induced phagocytosis. Increasing the number of replicates could clarify this potential effect. However, based on these results, we conclude that CO does not promote or inhibit the engulfment of latex beads.

A.



B.

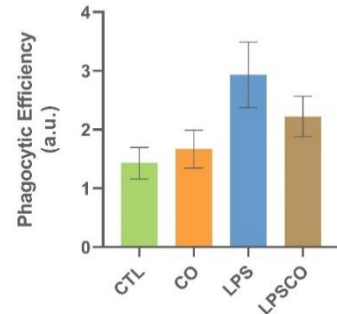


Figure 13 – Bead engulfment assays following protocol B. (A) Representative Z2 microscope images from the two assays (n=3) conducted (B4 and B5). Three to seven images were collected for each condition. Microglia is stained with phalloidin-AF555 (red) and incubated with fluorescent latex beads (green). Nuclei is stained with DAPI (blue). (B) Bar graph depicts the average phagocytic efficiency (Equation A described in Chapter 2) calculated for each condition. In each condition (control, CO-treated, LPS-treated and LPS+CO-treated), an average of 173, 142, 113 and 101 cells were analysed, respectively. Statistical significance between groups was calculated first, through a Kruskal-Wallis test, followed by Dunn’s multiple comparison test. P-value significance is represented by stars (*). P-values ≤ 0.05 (*), ≤ 0.01 (**), ≤ 0.001 (***) and ≤ 0.0001 (****), while non-significant relationships were omitted. Error bars illustrate SEM.

3.1.2. Phagocytosis protocol: apoptotic neuron engulfment assays

Phagocytosis allows microglia to maintain CNS homeostasis, namely, through clearance of dead cells and cellular debris. The previous bead engulfment assays allowed us to optimize experimental conditions, as well as gain some insight into CO's potential effects on this stage, under normal and inflammatory conditions. Thus, we sought to conduct similar assays, using neuronal debris, as to discern whether or not CO modulates the phagocytosis of dying neurons.

Firstly, in order to establish certain variables (neuron to microglial cell ratio and incubation time), we conducted two optimization assays according to the scheme depicted in *Table 7* in chapter 2, without CO administration or inflammation induction. These assays were analysed by live imaging analysis with an inverted light/fluorescent microscope.

Secondly, in order to evaluate CO's effects, we conducted a series of assays that were analysed through live imaging via fluorescence microscopy, as well as through flow cytometry, according to the scheme depicted in *Table 7* in chapter 2. In short, BV2 microglial cells received CO and/or LPS treatment, while apoptosis was induced in CAD neuronal cells using *t*-BHP. Neuronal debris were stained with TAMRA, while BV2 cells were stained with AF488-tagged IB4. Apoptotic neurons were then added to microglial cultures and incubated for 2 h. After the incubation period, samples were either analysed through live imaging or flow cytometry.

Live imaging

The first two assays served to optimize experimental variables (incubation time and neuron to microglia ratio) and the results of this optimization process are displayed in *Figure 14*. We tested two different ratios (1:1 and 1:2) as well as four different timepoints (1, 2, 3 and 5 h).

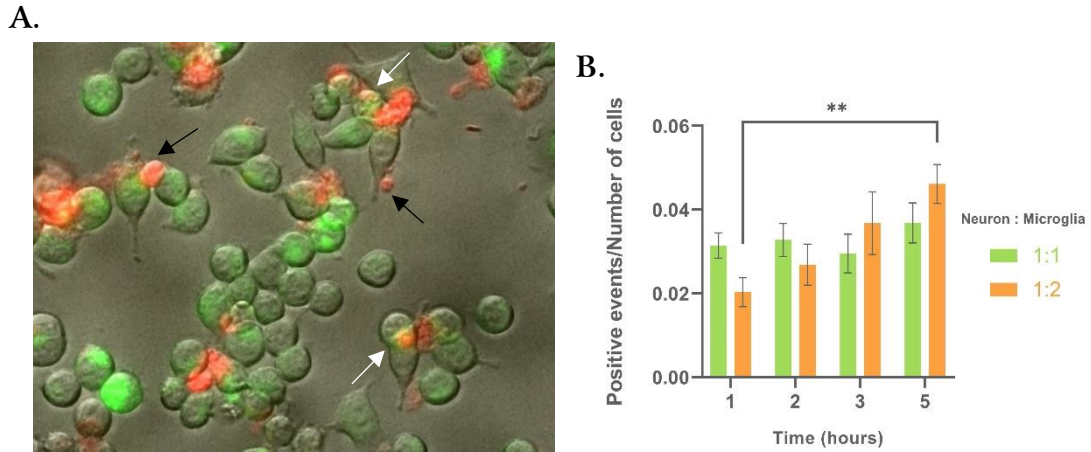


Figure 14 – Neuronal debris engulfment assays (optimization) – live imaging. (A) Inverted light/fluorescence microscope images. Microglia is stained with AF488-tagged IB4 (green), while neuronal debris are stained with TAMRA (red). Black arrows indicate non-engulfed neuronal debris, while white arrows indicate engulfed neuronal debris (positive event). (B) Optimization of variables – neuron to microglia ratio and incubation time. Bar graph depicts the average ratio of TAMRA-positive microglia to total number of microglial cells calculated for each condition. Two assays (n=2) conducted, and four to six images were analysed per condition, per assay. An average of 937 cells were analysed per condition. Statistical significance between groups was calculated first through an ordinary two-way ANOVA test, followed by Tukey’s multiple comparison test. P-value significance is represented by stars (*). P-values ≤ 0.05 (*), ≤ 0.01 (**), ≤ 0.001 (***) and ≤ 0.0001 (****), while non-significant relationships were omitted. Error bars illustrate SEM.

A 1:1 ratio (neuron to microglial cell) generated little to no difference in phagocytic rate throughout the different timepoints, while a 1:2 ratio led to its increase in a time-dependent manner. However, no statistical difference was found between the 2, 3 and 5 h timepoints. So, based on these results and for practical reasons, we established that the optimal conditions for future experiments would be to use a 1:2 neuron to microglia ratio and a 2 h incubation period.

Next, using the optimal conditions previously established, three more live imaging assays were conducted to assess CO’s effect on neuronal debris engulfment (Figure 15). Under inflammatory conditions, phagocytosis of neuronal debris was significantly inhibited. However, application of CO produced no significant effects on the engulfment of neuronal debris under an inflammatory context.

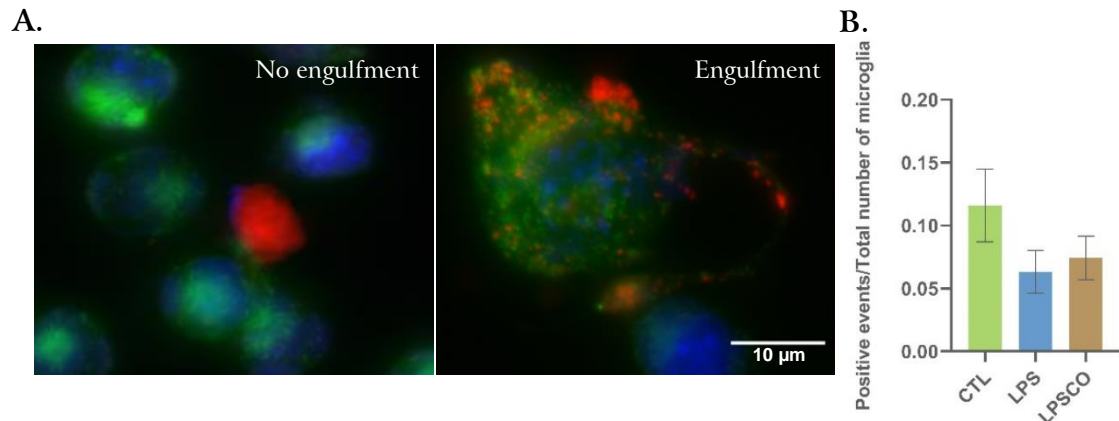


Figure 15 – Neuronal debris engulfment assays – live imaging. (A) Confocal images representing the difference between positive (engulfment of neuronal debris) and a negative event. Microglia is stained with AF488-tagged IB4 (green), neuronal debris are stained with TAMRA (red), and nuclei are stained with Hoechst (blue). (B) Bar graph depicts the average ratio of TAMRA-positive microglia to total number of microglia calculated for each condition. Five assays ($n=5$) were conducted, and four images were analysed per condition, per assay. While assessing the control, LPS and LPS+CO treated groups, an average of 735, 401 and 458 cells were analysed, respectively. Statistical significance between groups was calculated first through an ordinary one-way ANOVA test, followed by Tukey's multiple comparison test. P-value significance is represented by stars (*). P-values ≤ 0.05 (*), ≤ 0.01 (**), ≤ 0.001 (***) and ≤ 0.0001 (****), while non-significant relationships were omitted. Error bars illustrate SEM.

Flow cytometry

As to further validate the results obtained via live imaging, we conducted three assays according to the scheme described in *Table 7* (Chapter 2), followed by flow cytometry data analysis.

The protocol applied is described in the section 2.4.2. in chapter 2. Briefly, following the scheme depicted in *Table 7*, microglia were stained with AF-tagged IB4 (green), and neuronal debris were prepared and stained with TAMRA (red). Through the AF488 (green) and PE (red) channels, samples' fluorescence was measured by the cytometer. *Figure 16* illustrates the gating methodology applied to the data collected during these assays.

Forward scatter (FSC) correlates with cell size, while side scatter (SSC) is proportional to granularity/complexity. The first graph (*Figure 16A*) allowed us to visually separate cells from debris, based on FSC and SSC values. In order to separate single cells from doublets, we plotted the previously gated data by FSC area and FSC height (*Figure 16B*). Having a data pool of single cells, our next step was to separate them by their complexity and staining, which would allow us to distinguish between

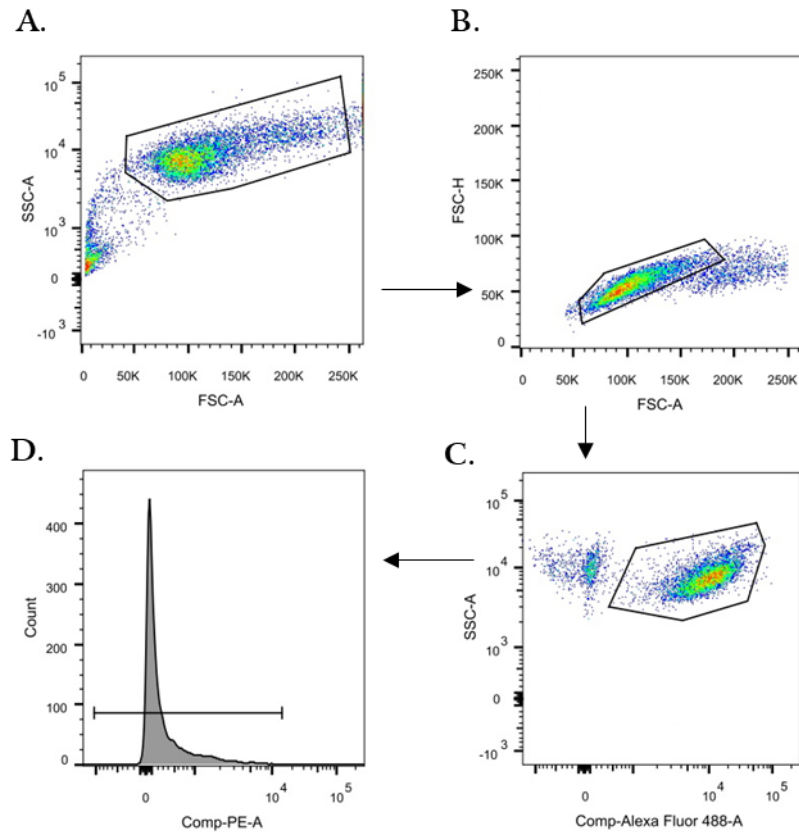


Figure 16 – Gating model utilized during flow cytometry assays. (A) Plot depicting event acquired by FSC area and SSC area. From this plot we were able to separate cells from debris. (B) Plot depicting the events gated in A by FSC area and FSC height. This allowed us to eliminate cell doublets and other events from our data pool. (C) Plot depicting the events previously gated in B by presence of AF488 fluorescence and SSC area. This made possible the separation of single microglial cells from non-IB4 stained events. (D) Distribution of TAMRA staining (neuronal debris presence) within the AF488⁺ population.

microglial cells and larger non-engulfed neuronal debris. For this, we plotted SSC area by presence of AF488 fluorescence (*Figure 16C*). Finally, in order to assess microglial phagocytic rate, we measured the median TAMRA fluorescence (through the PE channel) within our AF488⁺ events, previously gated (*Figure 16D*).

As we can see in *Figure 17*, the results did not emulate what was observed in the live imaging assays. In addition, it is observable that there was no significant difference in phagocytic rate between inflammatory and non-inflammatory conditions. However, unlike the results obtained from the live imaging assays, application of CO under both non-inflammatory and inflammatory conditions increased phagocytosis of neuronal debris by almost 1-fold.

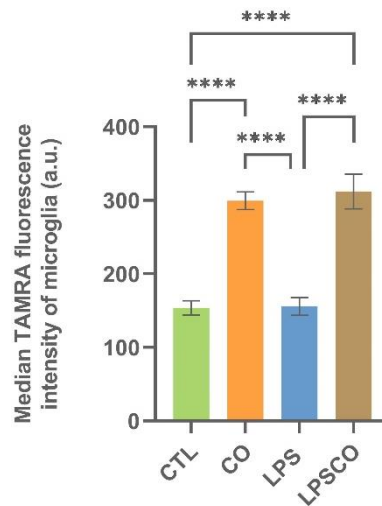


Figure 17 – Neuronal debris engulfment assays – flow cytometry. Bar graph depicts the average median TAMRA fluorescence of microglia (A488⁺ cells) registered for each condition. 10 000 events were analysed per condition. Statistical significance between groups was calculated first through an ordinary one-way ANOVA test, followed by Tukey's multiple comparison test. P-value significance is represented by stars (*). P-values ≤ 0.05 (*), ≤ 0.01 (**), ≤ 0.001 (***) and ≤ 0.0001 (****), while non-significant relationships were omitted. Error bars illustrate SEM.

3.2. Trafficking/Maturation stage

3.2.1. Phagocytosis protocol: LAMP-1 co-localization assessment

Cargo delivery to the lysosomes is essential for the efficiency of the phagocytic process. LAMP-1 is a lysosomal membrane protein that exists in abundance in these structures. In order to evaluate the successful phagosomal cargo delivery to lysosomes, we assessed the co-localization of LAMP-1 proteins with engulfed neuronal cargo (stained with TAMRA).

Four assays were conducted according to the protocol described in the second paragraph of section 2.4 in chapter 2. As a result of the application of this protocol, BV2 cells were stained with AF488-tagged IB4 (green), while neuronal debris were stained with TAMRA (yellow/orange). An immunofluorescence protocol (described in section 2.5 in chapter 2) was applied and, after fixing the samples, LAMP-1 proteins were stained with anti-LAMP-1 primary antibodies and, afterwards, AF647 secondary antibodies (red) and analysed via confocal microscopy. Results are displayed in *Figure 18*.

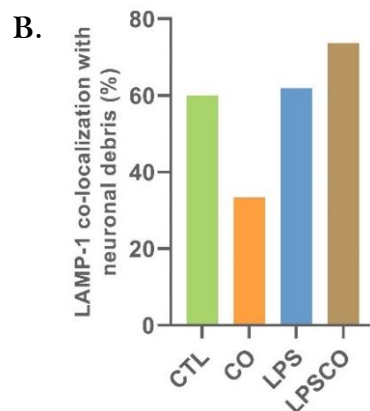
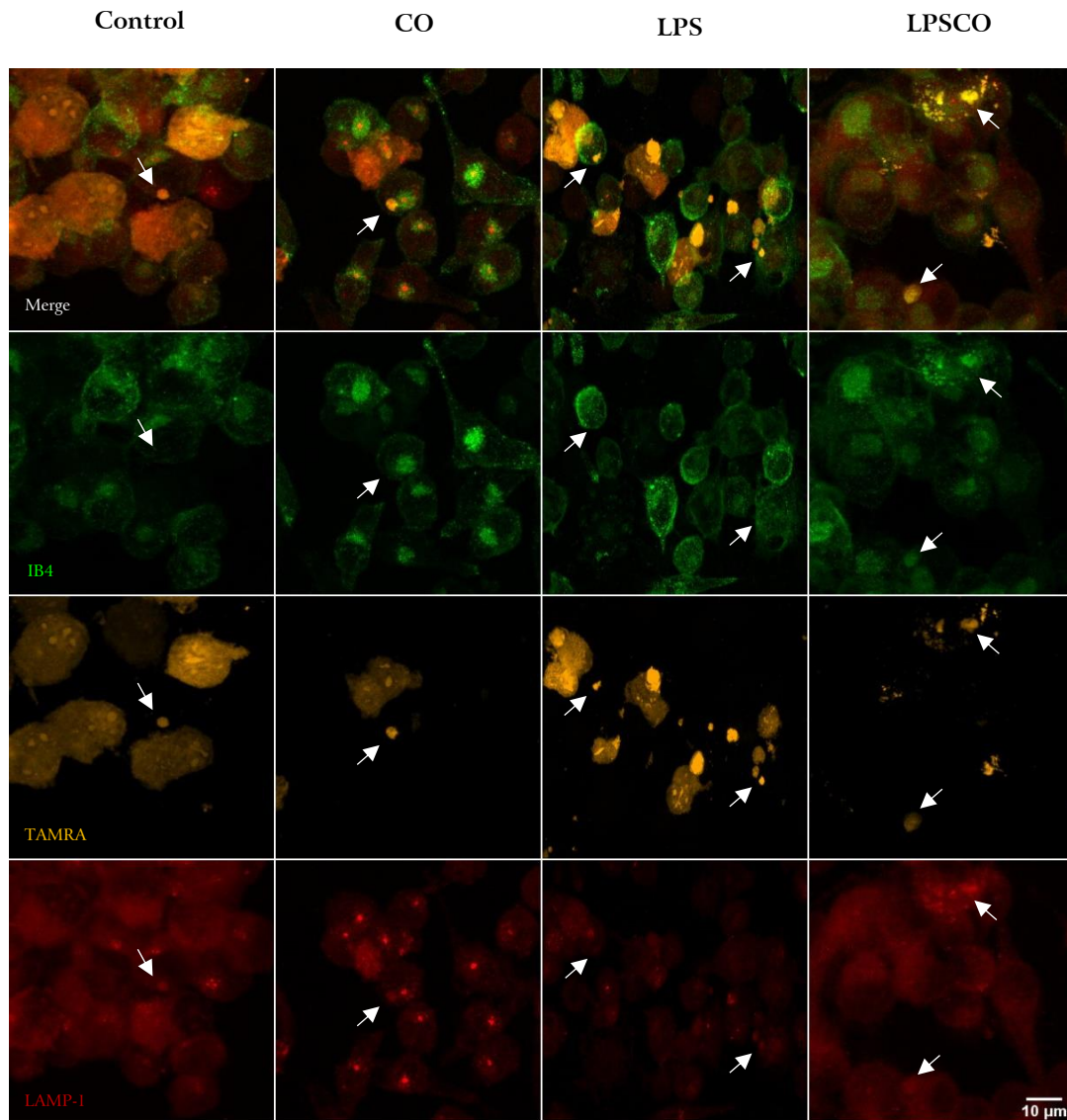


Figure 18 – LAMP-1 co-localization assays. (A) Representative confocal images collected from the four LAMP-1 staining assays (n=4) conducted. Four to ten images were analysed per condition. Microglia is stained with AF488-tagged IB4 (green), neurons are stained with TAMRA (orange), and LAMP-1 proteins are stained with anti-LAMP-1 primary antibodies and AF647 secondary antibodies (red). Arrows indicate LAMP-1 co-localization with engulfed neuronal debris. (B) Bar graph depicts the percentage of co-localization of LAMP-1 proteins with engulfed neuronal debris per condition. In the assessment of the control, CO-treated, LPS-treated and the LPS+CO-treated groups, 20, 15, 21 and 19 events (sum of all assays conducted) were analysed, respectively.

After assessing the number of engulfed neuronal debris within microglia, we then evaluated how many of these co-localized with LAMP-1 puncta formations. In *Figure 18B*, from the events accounted, under non-inflammatory conditions, we observed that CO, had less phagosomes fused with lysosomes (only 33.3%) in comparison to the control (60.0%), LPS-treated (61.9%) and LPS+CO-treated (73.7%). LPS+CO-treated group tended to exhibit more co-localization than all of the other conditions. Overall, there was not a statistically significant difference in the co-localization of LAMP-1 with neuronal debris in both inflammatory and non-inflammatory conditions. However, application of CO in non-inflammatory circumstances tended to exhibit decreased co-localization and, in inflammatory conditions, this effect was reversed. Nevertheless, this information serves as preliminary data and experiments must be repeated.

3.3. Degradation stage

3.3.1. Phagocytosis protocol: degradative function assessment

With the purpose of gaining some insight into how CO affects the degradation stage of microglial phagocytosis, we evaluated the degradation rate of DQ-BSA through its fluorescence emission over time. Hydrolysis of DQ-BSA generates fluorescent peptide products by dequenching and, as such, higher degradation of DQ-BSA leads to higher fluorescent emission. This way we are provided a direct insight to the cellular lysosomal activity and degradative capacity.

The protocol used is described in *Table 6* in chapter 2. Briefly, the experimental procedure consisted in adding DQ-BSA to microglial cultures and incubate it for 3 h. Afterwards, fluorescence readings at 645 nm were acquired every 10 min over a period of 4 h.

Three assays were conducted, and their results are displayed in *Figure 19*. Despite the large variability between the three assays conducted, a pattern is discernible. The application of CO under non-inflammatory conditions tends to promote more phagocytic cargo degradation in comparison to the LPS-treated groups.

We will need to conduct more assays in order to properly discern its impact on the degradation stage.

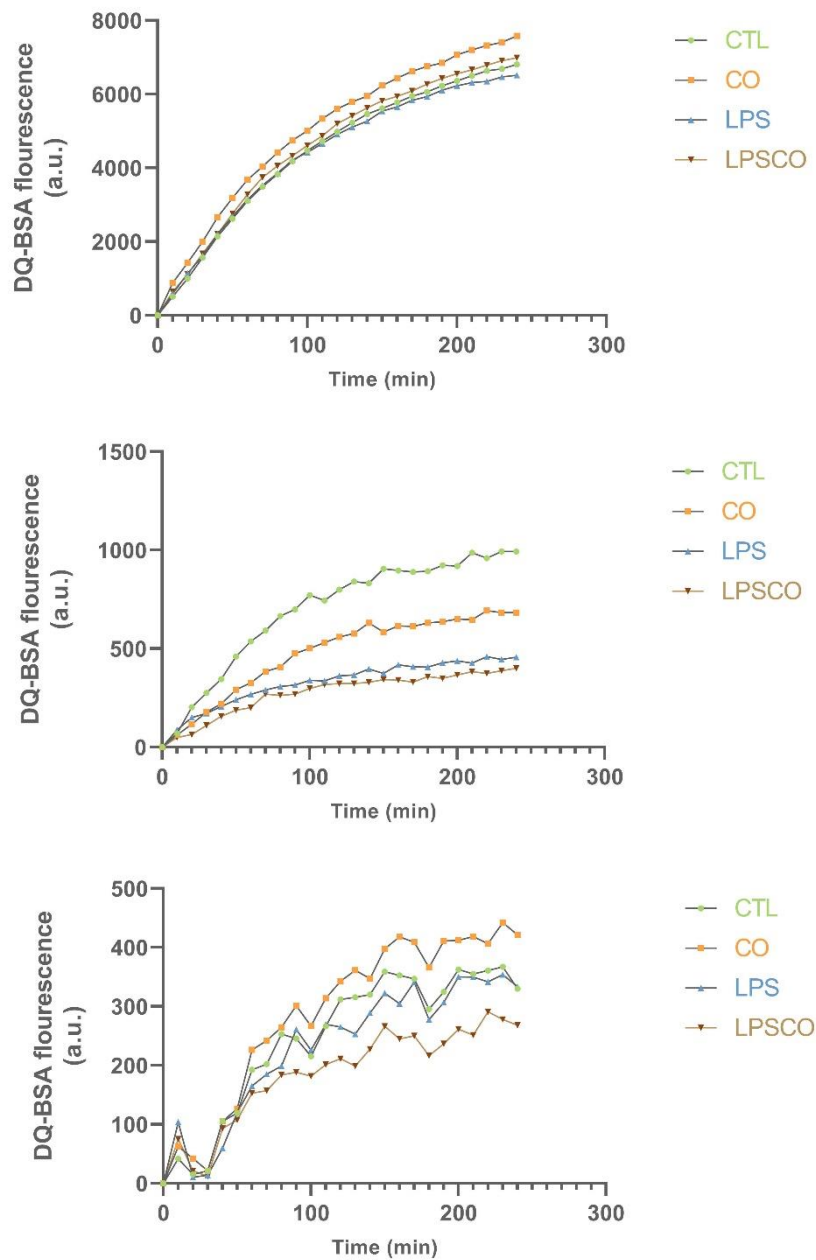


Figure 19 – DQ-BSA degradation assays. Connected scatter plots represent DQ-BSA fluorescence variation over time. Each plot represents one of the three assays conducted. Readings were acquired every 10 min throughout a 4 h time period at 645 nm. Cells were kept at approximately 37 °C during the acquisition.

Chapter 4

Discussion

Chapter 4 - Discussion

The CNS is a crucial structure in our organism and, as such, is under the constant vigilance of microglia, which methodically scan their surrounding microenvironment in search of pathological changes. Upon encountering such stimuli, they quickly become activated and mount an immune response in order to deal with the threat and restore CNS homeostasis. In addition to orchestrating immune responses, microglia are also responsible for synaptic plasticity management (through synaptic pruning), as well as clearance of dead cells and cellular debris.

As a means of effectively conducting the aforementioned functions, microglia resort to phagocytosis, a crucial step in the elimination of dead cells, pathogens, protein aggregates and cellular debris and, consequently, CNS homeostasis restoration. In a simplistic view, the phagocytic process can be divided into four stages – Recognition, Engulfment, Trafficking/Maturation and Degradation. Most of the research conducted into microglial phagocytosis mainly focuses on the first stage, and so the remaining stages are left poorly studied in comparison and are often assumed to be conducted in a similar, if not equal, manner as in other macrophages.

Throughout chapter 1, we have seen that CO can modulate key proteins in several signalling pathway related to immune response regulation, apoptosis prevention and the phagocytic process. Preliminary data gathered by our lab has revealed that CO enhances microglial engulfment of dead neurons, while preventing live ones from being phagocytosed. However, there is still much left unknown in terms of how CO operates to promote this effect on the phagocytic process.

In order to shed some light on this issue, the main goal of this thesis was to explore how CO can modulated microglial phagocytosis, specifically of dead/dying neurons, particularly in the last three stages of the phagocytic process. As to achieve such goal, we used a novel molybdenum-based CORM (ALF826), developed by Dr. Carlos Romão from ITQB/Proterris. Molybdenum-based CORMs are an exciting development, because, due to molybdenum's nature, these molecules seem to be more biocompatible than CORMs based around other transition metals, and thus represents

a step forward in the direction of creating safer and more effective CO-based therapeutic treatments.

4.1. Engulfment stage

4.1.1. Phagocytosis protocol optimization (beads)

Before studying the phagocytosis of neuronal debris, we started by first testing other target-particles (i.e., beads), as to gather more insight on the general effects of CO on the engulfment stage.

The first protocol we tried for the assessment of the engulfment stage, involved the use of 3 μm beads and did not work due to a low engulfment rate. Microglia were engulfing between 1 to 2 beads per phagocytic cell, and this led to low significance of the results acquired per assay. The low engulfment rate could be due to the relatively large size of the opsonized beads used in this protocol. Phagocytosis efficiency seems to be dependent on particle size, as concluded in the study conducted by Champion *et al.*¹⁹⁶, in which they used different macrophages and beads of varying sizes. In case of microglial cells, specifically BV2 cells, a study conducted by Majerova *et al.*¹⁹⁷, revealed that even the use of 2 μm latex beads resulted in low phagocytic efficiency. Bead-containing cells were only observable after 24 h. Furthermore, after 24 h, the control group only had 1.3% of bead-containing cells, while the LPS-treated had 2.3%. Other hypothetical causes for the low engulfment rate are that BV2 microglia cells are smaller and less phagocytic than the typical RAW macrophages used in similar experiments, or that they simply don't express Fc receptors abundantly enough to engulf these beads at a higher rate. One way we could have cleared this issue, was by testing the same conditions with a RAW 264.7 macrophage (murine cell line) and compare them to BV2 cells.

In addition, Cy5 staining was also relatively unsuccessful. It was observable in *Figure 11*, that excess Cy5 was able to accumulate within the cells and stain presumably engulfed beads. Furthermore, some clearly non-engulfed beads were left unstained by Cy5 antibodies. This could be due to technical errors during the execution of the bead

opsonization protocol applied for the assays, which would reduce Cy5 staining efficiency.

We then tried a different protocol using 1 μm fluorescent beads in order to circumvent the problem with bead size. With this protocol, we first established the optimal conditions (incubation time and concentration of beads), in order to assess the effects of CO application under inflammatory (LPS-induced) and non-inflammatory conditions. It has been shown in several studies that treating microglia with an inflammatory stimulus, like LPS, increases their bead engulfment rate^{198–200}. As expected, during our assays, we observed a tendency towards an increase in phagocytic efficiency, when under inflammatory conditions, in comparison with the control group (*Figure 13*). CO administration showed a tendency to reduce LPS-induced increase in engulfment rate. Similarly, to previous work done by our lab with primary microglia (unpublished), it was observed that LPS treatment increased bead engulfment and that treating microglia, under inflammatory conditions, with CO, attenuated this effect.

4.1.2. Phagocytosis protocol (apoptotic neurons)

Neuronal debris engulfment rate was assessed through two different methods – live cell imaging and flow cytometry.

Our live imaging analysis showed that CO, under inflammatory conditions did not affect neuronal debris engulfment in comparison to the controls (*Figure 15*). Nevertheless, there is a slight increase in microglial phagocytosis capacity following CO treatment, which is in accordance with previous data generated by our lab. Moreover, the flow cytometry assays revealed that CO was able to enhance neuronal debris engulfment under inflammatory and non-inflammatory conditions by almost 1-fold (*Figure 17*). This difference is likely due to the technical differences and, ultimately, the limitations each method possesses. Flow cytometry not only allows for the analysis of a larger volume of data (the analysis of more cells per assays), but it allows us to do so from a more unbiased standpoint. However, one must be cautious when gating the data acquired, as to avoid misleading data. On the other hand, one is

relatively able to distinguish a fully engulfed particle from a non-engulfed one in live imaging assays, but it lacks the unbiased standpoint and data volume afforded by flow cytometry.

The data acquired is in accordance with the preliminary data acquired by our lab (unpublished data), which revealed that CO enhanced microglial phagocytosis of neuronal debris. To the best of our knowledge, only one other study specifically addressed the impact CO has on microglial engulfment of apoptotic/dying neurons. However, it reported that CO led to a reduction in phagocytic rate in normal conditions and in acute inflammation (LPS-induced) ¹⁸⁸. The major difference in both studies is the time of contact between microglia and apoptotic neurons. In our assays, cells were only in contact for 2 h, whereas Scheiblich *et al.* ¹⁸⁸ kept the cells in co-culture for 24 h. After those 24 h, cells were fixed and analysed through confocal microscopy. The fact that they observed less phagocytosis (number of neuronal debris containing microglia/total number of microglia) when cells were treated with CO, could be due to a faster uptake and cargo degradation in comparison to the control, and not necessarily an inhibitory effect. Scheiblich *et al.* ¹⁸⁸ also reported that BV2 cell treatment with LPS (24 h prior incubation with neurons and no further LPS addition) resulted in an increase in neuronal debris engulfment (14.8%) in comparison to the control without any LPS administration (8.74%). However, our results show that, administration of LPS 24 h prior incubation with apoptotic neurons, had no significant change in comparison to the control. This disparity could be due to different methods applied (volume of data analysed) and co-incubation time.

Looking back to the results obtained in our bead engulfment assays, we were able to observe several differences between those results and the ones obtained with neuronal debris. We noticed that LPS, promoted the engulfment of latex beads, but showed no effect in the engulfment of apoptotic neurons. A study conducted by Shiratsuchi *et al.* ²⁰¹, reported a similar occurrence. They conducted an experiment where they were able to see the effect of LPS on the engulfment of apoptotic thymocytes by macrophages and, regardless of LPS-induced inflammation, they did not observe a difference in phagocytic rate. This could mean that LPS is able to upregulate elements involved in bead engulfment, but not in the engulfment of

apoptotic cells, meaning that these target particles are not engaged by microglia the same way (e.g., different receptors and/or engulfment mechanisms).

In summary, CO promotes neuronal debris-receptor binding and, consequently, neuronal debris engulfment by microglia. Furthermore, according to these and previous data, CO seems to reduce the engulfment of 1 μm beads, under inflammatory conditions. The differences observed between bead and neuronal debris engulfment under inflammatory conditions, could be due to different mechanisms being employed for their engulfment. Nevertheless, the fact that CO is able to modulate microglia in a way that it increases their apoptotic neuron engulfment rate seems to have a cytoprotective impact. By promoting apoptotic cell clearance, CO is thus contributing to CNS homeostasis.

4.2. Trafficking/maturation stage

After evaluating the engulfment of apoptotic neurons, we moved on to assessing the success rate of neuronal debris containing-phagosomes trafficking into lysosomes.

To the best of our knowledge, there are no studies reporting on CO's influence in phagosomal trafficking/maturation process in the context of microglial phagocytosis. CO has been shown to promote the upregulation of lysosome biogenesis-associated genes like cathepsin B, D, in addition to LAMP-1²⁰². Furthermore, CO gas treatment led to an increase in LAMP-1 mRNA expression, increased the LC3-II/LC3-I ratio and reduced bacterial load in mice lung tissue²⁰³. This would indicate that application of CO, under inflammatory conditions, promotes phagosome/endosome maturation.

In our co-localization assays of LAMP-1 proteins with engulfed neuronal debris (*Figure 18B*), it was observed that LPS-treatment did not influence co-localization relatively to the control group. However, under non-inflammatory conditions CO treatment produced a substantial decrease in comparison to all other groups (26.7%, 28.6% and 40.4% decrease in comparison to the control, LPS-treated and LPS+CO-treated groups, respectively). Since phagocytic stages cannot be analysed

independently, we must also take into consideration the conclusions drawn from our assessment of the engulfment stage. We saw that treating microglia cells with CO, in both inflammatory and non-inflammatory conditions, led to an increase of almost 1-fold in engulfment rate. So, in light of that information, we observed that:

- (1) Under non-inflammatory conditions, treating microglia with CO, led to lower neuronal-debris co-localization with LAMP-1 proteins. This can be interpreted in one of two ways: (a) the fact that co-localization is reduced, could mean that phagosomal trafficking/maturation is not upregulated proportionally to intake. In other words, in spite of intaking more cargo, microglia are not processing phagosomes at a proportional speed; or (b) the reduced co-localization observed could be due to faster cargo degradation, leading to less co-localizing events available for observance.
- (2) Under inflammatory conditions, the LPS+CO-treated group exhibited similar if not superior percentage of co-localization between neuronal debris and LAMP-1 proteins, in comparison with the other conditions. Now this can also be interpreted in one of two ways: (a) Addition of CO, under inflammatory conditions, promotes faster phagosomal processing; or (b) CO's effects on this stage are dependent on an inflammatory stimulus like LPS.

To properly address these issues, we could use a lysosomal inhibitor, like chloroquine, and then assess co-localization. In addition, studying phagosomal maturation and phagocytic flux markers are also an interesting option. To surmise, CO role in this stage is still uncertain, but its modulating capabilities do, in fact, impact phagosomal processing. Further experiments are needed to fully disclose its role within this stage in particular.

4.3. Degradation stage

4.3.1. Phagocytosis protocol (DQ-BSA)

As a means of gaining some insight to CO's effects on the degradation stage, we conducted three degradations assays with DQ-BSA.

As mentioned previously, CO promotes the expression of TFEB, LAMP-1 and cathepsins, which are key elements for optimal lysosomal activity and promotion of phagocytic cargo degradation. However, studies have shown CO in conjunction with LPS-induced inflammation, reduced dendritic cell's ability to degrade DQ-Ovalbumin (similar to DQ-BSA) ^{204,205}.

Despite the large variability between the assays we conducted, we did observe (*Figure 19*) a similar pattern to what is described in the literature. In LPS-treated groups we tended to observe less DQ-BSA degradation. However, under non-inflammatory conditions, CO tended to promote DQ-BSA degradation in comparison to the other groups. Further assays are needed to verify this trend and draw more solid conclusions on the matter, as well as assays assessing the degradation of neuronal debris engulfed by microglia. One way we can conduct the latter experiments is through flow cytometry assays. We could stain lysosomes with an undegradable dye, while staining neurons with a pH-sensitive dye and compare the ratio of degradable dye/undegradable dye between conditions. In addition, lysosomal pH measurement and cathepsin activity assays are viable ways of indirectly measuring the degradative capacity of lysosomes. Nonetheless, if this trend is true, it would seem that CO is able to upregulate microglia's ability to degrade engulfed cargo, under non-inflammatory conditions.

4.4. Final remarks

In conclusion, throughout this work we were able to discern that:

- (1) CO promotes neuronal debris engulfment by microglia

- (2) CO has an impact in phagosomal processing, both under inflammatory and non-inflammatory conditions. However, the exact nature of its role in this stage remains unknown.
- (3) Further assays are needed in order to ascertain CO's effect on neuronal debris degradation.

Looking back at what we know from the mechanisms involved in LAP (section 1.3.1, chapter 1) and adding the information we've gathered from these assays, one might speculate that CO is modulating Beclin-1 and NOX2, and, thus, promoting these effects.

Firstly, Beclin-1 has been shown to be critical for microglial engulfment of latex beads and A β ⁶⁹. Lee *et al.* ¹⁹¹ conducted a study where mice with properly functioning Beclin-1 (Beclin-1 ^{+/+}) were injured by caecal ligation puncture and upon being exposed to CO, they showed a significant improvement in survival rate when compared to the air-exposed control group. However, CO was unable to rescue Beclin-1-deficient mice (Beclin-1 ^{-/-}) survival rates. It was later shown in this study that CO promoted Beclin-1-dependent CD150 upregulation, an important receptor for bacteria clearance. Similarly, downregulation of Beclin-1 in microglial cells resulted, in impaired surface expression of CD36 and TREM2 ⁶⁹, two receptors that have been reported to mediate apoptotic cell engulfment. In addition, CO, by promoting CD36 cell surface expression, was able to increase microglial erythrophagocytosis and reduce neuronal damage ¹⁹⁰. Based on this information, CO could be promoting the expression and/or a faster recycling of receptors, by modulating Beclin-1 and thus facilitating the engulfment stage in the phagocytic process. In order to prove this, future experiments should be centred around, firstly, on whether or not neuronal debris are being engulfed via a LAP-like mechanism. Secondly, they should focus on the identification of the main receptors being used to bind neuronal debris and assessing their recycling rate and its dependency on Beclin-1's presence.

As for NOX2, CO is known for interacting with haem-containing proteins and, through such interaction, CO might be inhibiting ROS production via inhibition of NOX2 ²⁰⁶. Phagosome maturation is dependent, among other factors, in the

production of ROS and thus it would explain why we see some lagging phagosomes when we treat cell with CO, under non-inflammatory conditions. CO's effects on NOX2 under inflammatory conditions were likely overshadowed by LPS-triggered ROS production. For future experiments, in addition to evaluating NOX2 activity and ROS formation, it would be interesting to also look into PIP3 formation, LC3II/LC3I ratio as well as monitor the expression and/or activity of proteins involved in phagosome-lysosome fusion. This way we can achieve a more in-depth assessment of CO's impact on this specific stage.

All in all, CO seems to modulate microglia in a way that makes them more efficient phagocytes towards apoptotic neurons. By making microglia more efficient at apoptotic cell clearance, CO is thus promoting CNS homeostasis and cytoprotection.

Chapter 5

Conclusion

Chapter 5 - Conclusion

Microglia are key players in CNS homeostasis, namely through the clearance of dead cells, pathogens, protein aggregates and cellular debris through phagocytosis. As such, the interest in thematics surrounding microglia is growing rapidly. Administration of low doses of CO has been shown to exert salutary effects through the modulation of several key pathways related to immune response regulation, apoptosis prevention and the phagocytic process. Despite this growing interest in the field, there's a lack of research into the molecular mechanisms behind microglial phagocytosis and CO's role in it.

In order to start filling in the gaps, this thesis was designed as a starting point. Throughout this work we showed how CO is able to impact phagocytosis at the engulfment, trafficking/maturation and degradation stage (*Figure 20*). By modulating microglia in a way that it increases their apoptotic neuron engulfment rate, CO has a cytoprotective impact, favouring CNS homeostasis.

By the end of our work, we were able to answer the questions posed at the beginning and raised several others. Those will require a more in-depth assessment and will serve as guidelines for future experiments.

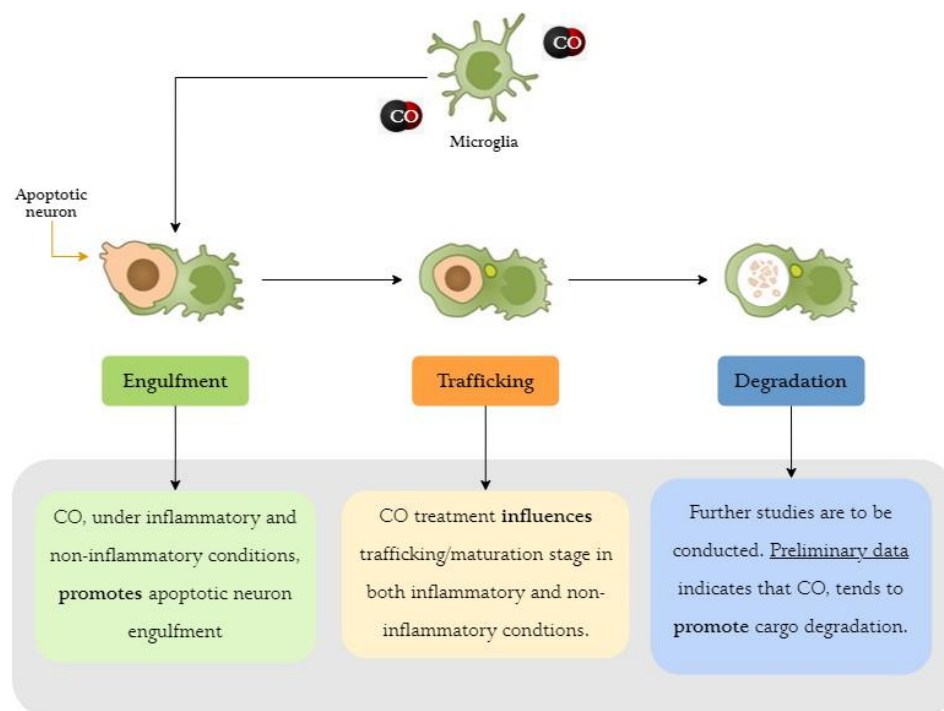


Figure 20 – Main conclusions from this thesis.

References

1. Hughes, J. T. The Edwin Smith Surgical Papyrus: an analysis of the first case reports of spinal cord injuries. *Spinal Cord* **26**, 71–82 (1988).
2. Breitenfeld, T., Jurasic, M. J. & Breitenfeld, D. Hippocrates: the forefather of neurology. *Neurol Sci* **35**, 1349–1352 (2014).
3. History of Neuroscience. <https://faculty.washington.edu/chudler/hist.html>.
4. Finkelstein, G. Mechanical neuroscience: Emil du Bois-Reymond's innovations in theory and practice. *Front. Syst. Neurosci.* **9**, (2015).
5. Parpura, V. & Verkhratsky, A. Neuroglia at the Crossroads of Homeostasis, Metabolism and Signalling: Evolution of the Concept. *ASN Neuro* **4**, AN20120019 (2012).
6. Scheurlein, H., Henschke, F. & Köckerling, F. Wilhelm von Waldeyer-Hartz—A Great Forefather: His Contributions to Anatomy with Particular Attention to “His” Fascia. *Front. Surg.* **4**, 74 (2017).
7. Breathnach, C. S. Charles Scott Sherrington's Integrative Action: a centenary notice. *JRSM* **97**, 34–36 (2004).
8. Schwiening, C. J. A brief historical perspective: Hodgkin and Huxley: Classical Perspectives. *The Journal of Physiology* **590**, 2571–2575 (2012).
9. Eriksson, P. S. *et al.* Neurogenesis in the adult human hippocampus. *Nat Med* **4**, 1313–1317 (1998).
10. Ludwig, P. E., Reddy, V. & Varacallo, M. Neuroanatomy, Neurons. in *StatPearls* (StatPearls Publishing, 2021).
11. *Neuroscience*. (Oxford University Press, 2018).
12. Mederos, S., González-Arias, C. & Perea, G. Astrocyte–Neuron Networks: A Multilane Highway of Signaling for Homeostatic Brain Function. *Front. Synaptic Neurosci.* **10**, 45 (2018).
13. Schousboe, A., Scafidi, S., Bak, L. K., Waagepetersen, H. S. & McKenna, M. C. Glutamate Metabolism in the Brain Focusing on Astrocytes. in *Glutamate and ATP at the Interface of Metabolism and Signaling in the Brain* (eds. Parpura, V., Schousboe, A. & Verkhratsky, A.) vol. 11 13–30 (Springer International Publishing, 2014).
14. Wang, X. F. & Cynader, M. S. Astrocytes Provide Cysteine to Neurons by Releasing Glutathione. *Journal of Neurochemistry* **74**, 1434–1442 (2002).
15. Deitmer, J. W., Theparambil, S. M., Ruminot, I., Noor, S. I. & Becker, H. M. Energy Dynamics in the Brain: Contributions of Astrocytes to Metabolism and pH Homeostasis. *Front. Neurosci.* **13**, 1301 (2019).
16. Bélanger, M., Allaman, I. & Magistretti, P. J. Brain Energy Metabolism: Focus on Astrocyte-Neuron Metabolic Cooperation. *Cell Metabolism* **14**, 724–738 (2011).
17. Baldwin, K. T. & Eroglu, C. Molecular mechanisms of astrocyte-induced synaptogenesis. *Current Opinion in Neurobiology* **45**, 113–120 (2017).
18. Winship, I. R., Plaa, N. & Murphy, T. H. Rapid Astrocyte Calcium Signals Correlate with Neuronal Activity and Onset of the Hemodynamic Response In Vivo. *Journal of Neuroscience* **27**, 6268–6272 (2007).
19. Pasti, L., Volterra, A., Pozzan, T. & Carmignoto, G. Intracellular Calcium Oscillations in Astrocytes: A Highly Plastic, Bidirectional Form of Communication between Neurons and Astrocytes *In Situ*. *J. Neurosci.* **17**, 7817–7830 (1997).
20. Fellin, T. *et al.* Neuronal Synchrony Mediated by Astrocytic Glutamate through Activation of Extrasynaptic NMDA Receptors. *Neuron* **43**, 729–743 (2004).
21. Scimemi, A. The Role of Astrocytes in Neurotransmitter Uptake and Brain Metabolism. in *Computational Glioscience* (eds. De Pittà, M. & Berry, H.) 309–328 (Springer International Publishing, 2019). doi:10.1007/978-3-030-00817-8_12.
22. Sofroniew, M. V. Astrogliosis. *Cold Spring Harb Perspect Biol* **7**, a020420 (2015).

23. Sierra, A. *et al.* The “Big-Bang” for modern glial biology: Translation and comments on Pío del Río-Hortega 1919 series of papers on microglia: 1919 Río-Hortega Papers on Microglia. *Glia* **64**, 1801–1840 (2016).
24. Herzog, C. *et al.* Rapid clearance of cellular debris by microglia limits secondary neuronal cell death after brain injury *in vivo*. *Development* **146**, dev174698 (2019).
25. Cunningham, C. L., Martinez-Cerdeno, V. & Noctor, S. C. Microglia Regulate the Number of Neural Precursor Cells in the Developing Cerebral Cortex. *Journal of Neuroscience* **33**, 4216–4233 (2013).
26. Neher, J. J. *et al.* Phagocytosis executes delayed neuronal death after focal brain ischemia. *Proceedings of the National Academy of Sciences* **110**, E4098–E4107 (2013).
27. Schafer, D. P. *et al.* Microglia Sculpt Postnatal Neural Circuits in an Activity and Complement-Dependent Manner. *Neuron* **74**, 691–705 (2012).
28. Wu, Y., Dissing-Olesen, L., MacVicar, B. A. & Stevens, B. Microglia: Dynamic Mediators of Synapse Development and Plasticity. *Trends in Immunology* **36**, 605–613 (2015).
29. Jurga, A. M., Paleczna, M. & Kuter, K. Z. Overview of General and Discriminating Markers of Differential Microglia Phenotypes. *Front. Cell. Neurosci.* **14**, 198 (2020).
30. Nimmerjahn, A. Resting Microglial Cells Are Highly Dynamic Surveillants of Brain Parenchyma in Vivo. *Science* **308**, 1314–1318 (2005).
31. Davalos, D. *et al.* ATP mediates rapid microglial response to local brain injury in vivo. *Nature Neuroscience* **8**, 752–758 (2005).
32. Ginhoux, F., Schultze, J. L., Murray, P. J., Ochando, J. & Biswas, S. K. New insights into the multidimensional concept of macrophage ontogeny, activation and function. *Nat Immunol* **17**, 34–40 (2016).
33. Dubbelaar, M. L., Kracht, L., Eggen, B. J. L. & Boddeke, E. W. G. M. The Kaleidoscope of Microglial Phenotypes. *Front. Immunol.* **9**, 1753 (2018).
34. Lyman, M., Lloyd, D. G., Ji, X., Vizcaychipi, M. P. & Ma, D. Neuroinflammation: The role and consequences. *Neuroscience Research* **79**, 1–12 (2014).
35. Mogi, M. *et al.* Interleukin (IL)-1 β , IL-2, IL-4, IL-6 and transforming growth factor- α levels are elevated in ventricular cerebrospinal fluid in juvenile parkinsonism and Parkinson’s disease. *Neuroscience Letters* **211**, 13–16 (1996).
36. Swardfager, W. *et al.* A Meta-Analysis of Cytokines in Alzheimer’s Disease. *Biological Psychiatry* **68**, 930–941 (2010).
37. Tang, Y. & Le, W. Differential Roles of M1 and M2 Microglia in Neurodegenerative Diseases. *Mol Neurobiol* **53**, 1181–1194 (2016).
38. Ledebor, A., Brevé, J. J., Poole, S., Tilders, F. J. & Van Dam, A. M. Interleukin-10, interleukin-4, and transforming growth factor-beta differentially regulate lipopolysaccharide-induced production of pro-inflammatory cytokines and nitric oxide in co-cultures of rat astroglial and microglial cells. *Glia* **30**, 134–142 (2000).
39. Zhao, W., Xie, W., Xiao, Q., Beers, D. R. & Appel, S. H. Protective effects of an anti-inflammatory cytokine, interleukin-4, on motoneuron toxicity induced by activated microglia. *J Neurochem* **99**, 1176–1187 (2006).
40. Patel, N. S. *et al.* Inflammatory cytokine levels correlate with amyloid load in transgenic mouse models of Alzheimer’s disease. *J Neuroinflammation* **2**, 9 (2005).
41. Lee, C. Y. D. & Landreth, G. E. The role of microglia in amyloid clearance from the AD brain. *J Neural Transm* **117**, 949–960 (2010).
42. Yang, W. *et al.* Aquaporin-4 mediates astrocyte response to β -amyloid. *Molecular and Cellular Neuroscience* **49**, 406–414 (2012).
43. Domínguez-Prieto, M., Velasco, A., Tabernero, A. & Medina, J. M. Endocytosis and Transcytosis of Amyloid- β Peptides by Astrocytes: A Possible Mechanism for Amyloid- β Clearance in Alzheimer’s Disease. *JAD* **65**, 1109–1124 (2018).
44. Koenigsknecht-Talboo, J. Microglial Phagocytosis Induced by Fibrillar β -Amyloid and IgGs Are Differentially Regulated by Proinflammatory Cytokines. *Journal of Neuroscience* **25**, 8240–8249 (2005).

45. Michelucci, A., Heurtaux, T., Grandbarbe, L., Morga, E. & Heuschling, P. Characterization of the microglial phenotype under specific pro-inflammatory and anti-inflammatory conditions: Effects of oligomeric and fibrillar amyloid- β . *Journal of Neuroimmunology* **210**, 3–12 (2009).
46. Hu, X. *et al.* Microglia/Macrophage Polarization Dynamics Reveal Novel Mechanism of Injury Expansion After Focal Cerebral Ischemia. *Stroke* **43**, 3063–3070 (2012).
47. Xiong, X. *et al.* Increased Brain Injury and Worsened Neurological Outcome in Interleukin-4 Knockout Mice After Transient Focal Cerebral Ischemia. *Stroke* **42**, 2026–2032 (2011).
48. Pérez-de Puig, I. *et al.* IL-10 Deficiency Exacerbates the Brain Inflammatory Response to Permanent Ischemia without Preventing Resolution of the Lesion. *J Cereb Blood Flow Metab* **33**, 1955–1966 (2013).
49. Janda, E., Boi, L. & Carta, A. R. Microglial Phagocytosis and Its Regulation: A Therapeutic Target in Parkinson's Disease? *Front. Mol. Neurosci.* **11**, 144 (2018).
50. Plaza-Zabala, A., Sierra-Torre, V. & Sierra, A. Autophagy and Microglia: Novel Partners in Neurodegeneration and Aging. *IJMS* **18**, 598 (2017).
51. Kigerl, K. A., de Rivero Vaccari, J. P., Dietrich, W. D., Popovich, P. G. & Keane, R. W. Pattern recognition receptors and central nervous system repair. *Experimental Neurology* **258**, 5–16 (2014).
52. Wu, L.-J., Vadakkan, K. I. & Zhuo, M. ATP-induced chemotaxis of microglial processes requires P2Y receptor-activated initiation of outward potassium currents. *Glia* **55**, 810–821 (2007).
53. Honda, S. *et al.* Extracellular ATP or ADP Induce Chemotaxis of Cultured Microglia through G_{i/o}-Coupled P2Y Receptors. *J. Neurosci.* **21**, 1975–1982 (2001).
54. Segawa, K. & Nagata, S. An Apoptotic 'Eat Me' Signal: Phosphatidylserine Exposure. *Trends in Cell Biology* **25**, 639–650 (2015).
55. Nomura, K., Vilalta, A., Allendorf, D. H., Hornik, T. C. & Brown, G. C. Activated Microglia Desialylate and Phagocytose Cells via Neuraminidase, Galectin-3, and Mer Tyrosine Kinase. *J.I.* **198**, 4792–4801 (2017).
56. Sapar, M. L. *et al.* Phosphatidylserine Externalization Results from and Causes Neurite Degeneration in Drosophila. *Cell Reports* **24**, 2273–2286 (2018).
57. Shin, H.-W. & Takatsu, H. Phosphatidylserine exposure in living cells. *Critical Reviews in Biochemistry and Molecular Biology* **55**, 166–178 (2020).
58. Hornik, T. C., Vilalta, A. & Brown, G. C. Activated microglia cause reversible apoptosis of pheochromocytoma cells, inducing their cell death by phagocytosis. *Journal of Cell Science* jcs.174631 (2015) doi:10.1242/jcs.174631.
59. Scott-Hewitt, N. *et al.* Local externalization of phosphatidylserine mediates developmental synaptic pruning by microglia. *EMBO J* **39**, (2020).
60. Li, T. *et al.* A splicing isoform of GPR56 mediates microglial synaptic refinement via phosphatidylserine binding. *EMBO J* **39**, (2020).
61. Lemke, G. Phosphatidylserine Is the Signal for TAM Receptors and Their Ligands. *Trends in Biochemical Sciences* **42**, 738–748 (2017).
62. Lehrman, E. K. *et al.* CD47 Protects Synapses from Excess Microglia-Mediated Pruning during Development. *Neuron* **100**, 120-134.e6 (2018).
63. Ding, X. *et al.* Loss of microglial SIRP α promotes synaptic pruning in preclinical models of neurodegeneration. *Nat Commun* **12**, 2030 (2021).
64. Klaus, C., Liao, H., Allendorf, D. H., Brown, G. C. & Neumann, H. Sialylation acts as a checkpoint for innate immune responses in the central nervous system. *Glia* **69**, 1619–1636 (2021).
65. Safaiyan, S. *et al.* Age-related myelin degradation burdens the clearance function of microglia during aging. *Nat Neurosci* **19**, 995–998 (2016).
66. Galloway, D. A., Phillips, A. E. M., Owen, D. R. J. & Moore, C. S. Phagocytosis in the Brain: Homeostasis and Disease. *Front. Immunol.* **10**, 790 (2019).

67. Gabandé-Rodríguez, E., Keane, L. & Capasso, M. Microglial phagocytosis in aging and Alzheimer's disease. *J Neurosci Res* **98**, 284–298 (2020).
68. Ferreira, S. A. & Romero-Ramos, M. Microglia Response During Parkinson's Disease: Alpha-Synuclein Intervention. *Front. Cell. Neurosci.* **12**, 247 (2018).
69. Lucin, K. M. *et al.* Microglial Beclin 1 Regulates Retromer Trafficking and Phagocytosis and Is Impaired in Alzheimer's Disease. *Neuron* **79**, 873–886 (2013).
70. Heckmann, B. L. *et al.* LC3-Associated Endocytosis Facilitates β -Amyloid Clearance and Mitigates Neurodegeneration in Murine Alzheimer's Disease. *Cell* **178**, 536–551.e14 (2019).
71. Hickman, S. E., Allison, E. K. & El Khoury, J. Microglial Dysfunction and Defective - Amyloid Clearance Pathways in Aging Alzheimer's Disease Mice. *Journal of Neuroscience* **28**, 8354–8360 (2008).
72. Choi, I. *et al.* Microglia clear neuron-released α -synuclein via selective autophagy and prevent neurodegeneration. *Nat Commun* **11**, 1386 (2020).
73. Pinto, M. V. & Fernandes, A. Microglial Phagocytosis—Rational but Challenging Therapeutic Target in Multiple Sclerosis. *IJMS* **21**, 5960 (2020).
74. Heckmann, B. L. & Green, D. R. LC3-associated phagocytosis at a glance. *J Cell Sci* **132**, jcs222984 (2019).
75. Nakamura, S. *et al.* Suppression of autophagic activity by Rubicon is a signature of aging. *Nat Commun* **10**, 847 (2019).
76. Martinez, J. *et al.* Molecular characterization of LC3-associated phagocytosis reveals distinct roles for Rubicon, NOX2 and autophagy proteins. *Nat Cell Biol* **17**, 893–906 (2015).
77. Yang, C.-S. *et al.* Autophagy Protein Rubicon Mediates Phagocytic NADPH Oxidase Activation in Response to Microbial Infection or TLR Stimulation. *Cell Host & Microbe* **11**, 264–276 (2012).
78. Martinez, J. *et al.* Noncanonical autophagy inhibits the autoinflammatory, lupus-like response to dying cells. *Nature* **533**, 115–119 (2016).
79. Matsunaga, K. *et al.* Two Beclin 1-binding proteins, Atg14L and Rubicon, reciprocally regulate autophagy at different stages. *Nat Cell Biol* **11**, 385–396 (2009).
80. Sun, Q., Westphal, W., Wong, K. N., Tan, I. & Zhong, Q. Rubicon controls endosome maturation as a Rab7 effector. *Proceedings of the National Academy of Sciences* **107**, 19338–19343 (2010).
81. Shahraz, A. *et al.* Phagocytosis-related NADPH oxidase 2 subunit gp91phox contributes to neurodegeneration after repeated systemic challenge with lipopolysaccharides. *Glia* **69**, 137–150 (2021).
82. Chen, J. Heme oxygenase in neuroprotection: from mechanisms to therapeutic implications. *Reviews in the Neurosciences* **25**, (2014).
83. Cuadrado, A. & Rojo, A. Heme Oxygenase-1 as a Therapeutic Target in Neurodegenerative Diseases and Brain Infections. *CPD* **14**, 429–442 (2008).
84. Doré, S. *et al.* Heme oxygenase-2 is neuroprotective in cerebral ischemia. *Mol Med* **5**, 656–663 (1999).
85. Tenhunen, R., Marver, H. S. & Schmid, R. The enzymatic conversion of heme to bilirubin by microsomal heme oxygenase. *Proceedings of the National Academy of Sciences* **61**, 748–755 (1968).
86. Mccoubrey, W. K., Huang, T. J. & Maines, M. D. Isolation and Characterization of a cDNA from the Rat Brain that Encodes Hemoprotein Heme Oxygenase-3. *Eur J Biochem* **247**, 725–732 (1997).
87. Wang, G. *et al.* Time course of heme oxygenase-1 and oxidative stress after experimental intracerebral hemorrhage. *Acta Neurochir* **153**, 319–325 (2011).
88. Li, L., Li, C.-M., Wu, J., Huang, S. & Wang, G.-L. Heat shock protein 32/heme oxygenase-1 protects mouse Sertoli cells from hyperthermia-induced apoptosis by CO activation of sGC signalling pathways: Hsp32/HO-1 as a protective factor in Sertoli cells. *Cell Biol Int* **38**, 64–71 (2014).

89. Sutherland, B. A. *et al.* Cerebral heme oxygenase 1 and 2 spatial distribution is modulated following injury from hypoxia–ischemia and middle cerebral artery occlusion in rats. *Neuroscience Research* **65**, 326–334 (2009).
90. Allanson, M. & Reeve, V. E. Immunoprotective UVA (320–400 nm) Irradiation Upregulates Heme Oxygenase-1 in the Dermis and Epidermis of Hairless Mouse Skin. *Journal of Investigative Dermatology* **122**, 1030–1036 (2004).
91. Tyrrell, R. M. Solar Ultraviolet A Radiation: An Oxidizing Skin Carcinogen that Activates Heme Oxygenase-1. *Antioxidants & Redox Signaling* **6**, 835–840 (2004).
92. Willis, D. Expression and modulatory effects of heme oxygenase in acute inflammation in the rat. *Inflamm Res* **44**, S218–S220 (1995).
93. Di Pietro, C., Öz, H. H., Murray, T. S. & Bruscia, E. M. Targeting the Heme Oxygenase 1/Carbon Monoxide Pathway to Resolve Lung Hyper-Inflammation and Restore a Regulated Immune Response in Cystic Fibrosis. *Front. Pharmacol.* **11**, 1059 (2020).
94. Dawn, B. & Bolli, R. HO-1 induction by HIF-1: a new mechanism for delayed cardioprotection? *American Journal of Physiology-Heart and Circulatory Physiology* **289**, H522–H524 (2005).
95. Lee, P. J. *et al.* Hypoxia-inducible Factor-1 Mediates Transcriptional Activation of the Heme Oxygenase-1 Gene in Response to Hypoxia. *Journal of Biological Chemistry* **272**, 5375–5381 (1997).
96. Lin, J. H.-C., Villalon, P., Martasek, P. & Abraham, N. G. Regulation of heme oxygenase gene expression by cobalt in rat liver and kidney. *Eur J Biochem* **192**, 577–582 (1990).
97. Min, K.-S. *et al.* Hydrogen Peroxide Induces Heme Oxygenase–1 and Dentin Sialophosphoprotein mRNA in Human Pulp Cells. *Journal of Endodontics* **34**, 983–989 (2008).
98. Nose, K. *et al.* Transcriptional activation of early-response genes by hydrogen peroxide in a mouse osteoblastic cell line. *Eur J Biochem* **201**, 99–106 (1991).
99. Foresti, R., Clark, J. E., Green, C. J. & Motterlini, R. Thiol Compounds Interact with Nitric Oxide in Regulating Heme Oxygenase-1 Induction in Endothelial Cells. *Journal of Biological Chemistry* **272**, 18411–18417 (1997).
100. Takahashi, K., Hara, E., Suzuki, H., Sasano, H. & Shibahara, S. Expression of Heme Oxygenase Isozyme mRNAs in the Human Brain and Induction of Heme Oxygenase-1 by Nitric Oxide Donors. *Journal of Neurochemistry* **67**, 482–489 (2002).
101. Unno, K. *et al.* Increase in Basal Level of Hsp70, Consisting Chiefly of Constitutively Expressed Hsp70 (Hsc70) in Aged Rat Brain. *The Journals of Gerontology Series A: Biological Sciences and Medical Sciences* **55**, B329–B335 (2000).
102. Hirose, W., Ikematsu, K. & Tsuda, R. Age-associated increases in heme oxygenase-1 and ferritin immunoreactivity in the autopsied brain. *Legal Medicine* **5**, S360–S366 (2003).
103. Carratu, P., Pourcyrus, M., Fedinec, A., Leffler, C. W. & Parfenova, H. Endogenous heme oxygenase prevents impairment of cerebral vascular functions caused by seizures. *American Journal of Physiology-Heart and Circulatory Physiology* **285**, H1148–H1157 (2003).
104. Maines, M. D. THE HEME OXYGENASE SYSTEM: A Regulator of Second Messenger Gases. *Annu. Rev. Pharmacol. Toxicol.* **37**, 517–554 (1997).
105. Raju, V. S., McCoubrey, W. K. & Maines, M. D. Regulation of heme oxygenase-2 by glucocorticoids in neonatal rat brain: characterization of a functional glucocorticoid response element. *Biochimica et Biophysica Acta (BBA) - Gene Structure and Expression* **1351**, 89–104 (1997).
106. Maines, M. D., Eke, B. C. & Zhao, X. Corticosterone promotes increased heme oxygenase-2 protein and transcript expression in the newborn rat brain. *Brain Research* **722**, 83–94 (1996).

107. Shiels, R. G. *et al.* Biliverdin and bilirubin sulfonate inhibit monosodium urate induced sterile inflammation in the rat. *European Journal of Pharmaceutical Sciences* **155**, 105546 (2020).
108. Lee, Y. *et al.* Hyaluronic acid–bilirubin nanomedicine for targeted modulation of dysregulated intestinal barrier, microbiome and immune responses in colitis. *Nat. Mater.* **19**, 118–126 (2020).
109. Gundamaraju, R., Vemuri, R., Chong, W. C., Bulmer, A. C. & Eri, R. Bilirubin Attenuates ER Stress-Mediated Inflammation, Escalates Apoptosis and Reduces Proliferation in the LS174T Colonic Epithelial Cell Line. *Int. J. Med. Sci.* **16**, 135–144 (2019).
110. Babu, D., Motterlini, R. & Lefebvre, R. A. CO and CO-releasing molecules (CO-RMs) in acute gastrointestinal inflammation. *British Journal of Pharmacology* **172**, 1557–1573 (2015).
111. Bainbridge, S. A., Belkacemi, L., Dickinson, M., Graham, C. H. & Smith, G. N. Carbon Monoxide Inhibits Hypoxia/Reoxygenation-Induced Apoptosis and Secondary Necrosis in Syncytiotrophoblast. *The American Journal of Pathology* **169**, 774–783 (2006).
112. Lee, H. & Choi, Y. Regenerative Effects of Heme Oxygenase Metabolites on Neuroinflammatory Diseases. *IJMS* **20**, 78 (2018).
113. Muñoz-Sánchez, J. & Cháñez-Cárdenas, M. E. A Review on Hemoxygenase-2: Focus on Cellular Protection and Oxygen Response. *Oxidative Medicine and Cellular Longevity* **2014**, 1–16 (2014).
114. Ryter, S. W., Alam, J. & Choi, A. M. K. Heme Oxygenase-1/Carbon Monoxide: From Basic Science to Therapeutic Applications. *Physiological Reviews* **86**, 583–650 (2006).
115. Dennery, P. A. Signaling Function of Heme Oxygenase Proteins. *Antioxidants & Redox Signaling* **20**, 1743–1753 (2014).
116. Shibahara, S., Han, F., Li, B. & Takeda, K. Hypoxia and Heme Oxygenases: Oxygen Sensing and Regulation of Expression. *Antioxidants & Redox Signaling* **9**, 2209–2226 (2007).
117. Otterbein, L. E. & Choi, A. M. K. Heme oxygenase: colors of defense against cellular stress. *American Journal of Physiology-Lung Cellular and Molecular Physiology* **279**, L1029–L1037 (2000).
118. Beard, J. L., Connor, J. R. & Jones, B. C. Iron in the Brain. *Nutrition Reviews* **51**, 157–170 (2009).
119. Balla, J. *et al.* Heme, heme oxygenase and ferritin in vascular endothelial cell injury. *Mol. Nutr. Food Res.* **49**, 1030–1043 (2005).
120. Eisenstein, R. S., Garcia-Mayol, D., Pettingell, W. & Munro, H. N. Regulation of ferritin and heme oxygenase synthesis in rat fibroblasts by different forms of iron. *Proceedings of the National Academy of Sciences* **88**, 688–692 (1991).
121. Stocker, R., Yamamoto, Y., McDonagh, A., Glazer, A. & Ames, B. Bilirubin is an antioxidant of possible physiological importance. *Science* **235**, 1043–1046 (1987).
122. Baranano, D. E., Rao, M., Ferris, C. D. & Snyder, S. H. Biliverdin reductase: A major physiologic cytoprotectant. *Proceedings of the National Academy of Sciences* **99**, 16093–16098 (2002).
123. Dore, S. *et al.* Bilirubin, formed by activation of heme oxygenase-2, protects neurons against oxidative stress injury. *Proceedings of the National Academy of Sciences* **96**, 2445–2450 (1999).
124. Dennery, P. A., McDonagh, A. F., Spitz, D. R., Rodgers, P. A. & Stevenson, D. K. Hyperbilirubinemia results in reduced oxidative injury in neonatal Gunn rats exposed to hyperoxia. *Free Radical Biology and Medicine* **19**, 395–404 (1995).
125. Perlstein, T. S., Pande, R. L., Creager, M. A., Weuve, J. & Beckman, J. A. Serum Total Bilirubin Level, Prevalent Stroke, and Stroke Outcomes: NHANES 1999–2004. *The American Journal of Medicine* **121**, 781–788.e1 (2008).
126. Djoussé, L. *et al.* Total serum bilirubin and risk of cardiovascular disease in the Framingham offspring study. *The American Journal of Cardiology* **87**, 1196–1200 (2001).

127. Maghzal, G. J., Leck, M.-C., Collinson, E., Li, C. & Stocker, R. Limited Role for the Bilirubin-Biliverdin Redox Amplification Cycle in the Cellular Antioxidant Protection by Biliverdin Reductase. *Journal of Biological Chemistry* **284**, 29251–29259 (2009).
128. McDonagh, A. F. The biliverdin–bilirubin antioxidant cycle of cellular protection: Missing a wheel? *Free Radical Biology and Medicine* **49**, 814–820 (2010).
129. Yu, Y. *et al.* A rat RNA-Seq transcriptomic BodyMap across 11 organs and 4 developmental stages. *Nat Commun* **5**, 3230 (2014).
130. Yue, F. *et al.* A comparative encyclopedia of DNA elements in the mouse genome. *Nature* **515**, 355–364 (2014).
131. Toxicological Profile for Carbon Monoxide. 347.
132. Bernard, C. *Leçons sur les effets des substances toxiques et médicamenteuses / par M. Claude Bernard.* (J.-B. Baillière et Fils [and 3 others], 1857). doi:10.5962/bhl.title.1834.
133. Hampson, N. B., Piantadosi, C. A., Thom, S. R. & Weaver, L. K. Practice Recommendations in the Diagnosis, Management, and Prevention of Carbon Monoxide Poisoning. *Am J Respir Crit Care Med* **186**, 1095–1101 (2012).
134. Alonso, J.-R., Cardellach, F., López, S., Casademont, J. & Miró, O. Carbon monoxide specifically inhibits cytochrome c oxidase of human mitochondrial respiratory chain. *Pharmacol Toxicol* **93**, 142–146 (2003).
135. Takano, T. *et al.* Direct effects of carbon monoxide on cardiac function. *Int. Arch Occup Environ Health* **49**, 35–40 (1981).
136. Ryter, S. W. & Choi, A. M. K. Targeting heme oxygenase-1 and carbon monoxide for therapeutic modulation of inflammation. *Translational Research* **167**, 7–34 (2016).
137. Figueiredo-Pereira, C., Dias-Pedroso, D., Soares, N. L. & Vieira, H. L. A. CO-mediated cytoprotection is dependent on cell metabolism modulation. *Redox Biology* **32**, 101470 (2020).
138. Boczkowski, J., Poderoso, J. J. & Motterlini, R. CO–metal interaction: vital signaling from a lethal gas. *Trends in Biochemical Sciences* **31**, 614–621 (2006).
139. Kung, Y. & Drennan, C. L. A role for nickel–iron cofactors in biological carbon monoxide and carbon dioxide utilization. *Current Opinion in Chemical Biology* **15**, 276–283 (2011).
140. Desmard, M., Amara, N., Lanone, S., Motterlini, R. & Boczkowski, J. Carbon monoxide reduces the expression and activity of matrix metalloproteinases 1 and 2 in alveolar epithelial cells. *Cell Mol Biol (Noisy-le-grand)* **51**, 403–408 (2005).
141. Zhang, H., Boulanger, M. J., Mauk, A. G. & Murphy, M. E. P. Carbon Monoxide Binding to Copper-Containing Nitrite Reductase from *Alcaligenes faecalis* †. *J. Phys. Chem. B* **104**, 10738–10742 (2000).
142. Ma, X., Sayed, N., Beuve, A. & van den Akker, F. NO and CO differentially activate soluble guanylyl cyclase via a heme pivot-bend mechanism. *EMBO J* **26**, 578–588 (2007).
143. Foresti, R. *et al.* Vasoactive properties of CORM-3, a novel water-soluble carbon monoxide-releasing molecule: Vasorelaxant properties of CORM-3. *British Journal of Pharmacology* **142**, 453–460 (2004).
144. Boehning, D. *et al.* Carbon Monoxide Neurotransmission Activated by CK2 Phosphorylation of Heme Oxygenase-2. *Neuron* **40**, 129–137 (2003).
145. Pae, H.-O. *et al.* Carbon Monoxide Produced by Heme Oxygenase-1 Suppresses T Cell Proliferation via Inhibition of IL-2 Production. *J Immunol* **172**, 4744–4751 (2004).
146. Otterbein, L. E. *et al.* Carbon monoxide has anti-inflammatory effects involving the mitogen-activated protein kinase pathway. *Nat Med* **6**, 422–428 (2000).
147. Brouard, S. *et al.* Carbon Monoxide Generated by Heme Oxygenase 1 Suppresses Endothelial Cell Apoptosis. *Journal of Experimental Medicine* **192**, 1015–1026 (2000).
148. Tongers, J. Heme oxygenase-1 inhibition of MAP kinases, calcineurin/NFAT signaling, and hypertrophy in cardiac myocytes. *Cardiovascular Research* **63**, 545–552 (2004).

149. Taillé, C., El-Benna, J., Lanone, S., Boczkowski, J. & Motterlini, R. Mitochondrial Respiratory Chain and NAD(P)H Oxidase Are Targets for the Antiproliferative Effect of Carbon Monoxide in Human Airway Smooth Muscle. *Journal of Biological Chemistry* **280**, 25350–25360 (2005).
150. Morse, D. *et al.* Suppression of Inflammatory Cytokine Production by Carbon Monoxide Involves the JNK Pathway and AP-1. *Journal of Biological Chemistry* **278**, 36993–36998 (2003).
151. Kim, S.-K. *et al.* Carbon monoxide decreases interleukin-1 β levels in the lung through the induction of pyrrolidone. *Cell Mol Immunol* **14**, 349–359 (2017).
152. Choi, Y. K. *et al.* Carbon Monoxide Promotes VEGF Expression by Increasing HIF-1 α Protein Level via Two Distinct Mechanisms, Translational Activation and Stabilization of HIF-1 α Protein. *Journal of Biological Chemistry* **285**, 32116–32125 (2010).
153. Bilban, M. *et al.* Carbon Monoxide Orchestrates a Protective Response through PPAR γ . *Immunity* **24**, 601–610 (2006).
154. Xie, Z. *et al.* Pretreatment of Mouse Neural Stem Cells with Carbon Monoxide-Releasing Molecule-2 Interferes with NF- κ B p65 Signaling and Suppresses Iron Overload-Induced Apoptosis. *Cell Mol Neurobiol* **36**, 1343–1351 (2016).
155. Wang, P. *et al.* Carbon Monoxide Improves Neurologic Outcomes by Mitochondrial Biogenesis after Global Cerebral Ischemia Induced by Cardiac Arrest in Rats. *Int. J. Biol. Sci.* **12**, 1000–1009 (2016).
156. Almeida, A. S., Queiroga, C. S. F., Sousa, M. F. Q., Alves, P. M. & Vieira, H. L. A. Carbon Monoxide Modulates Apoptosis by Reinforcing Oxidative Metabolism in Astrocytes. *Journal of Biological Chemistry* **287**, 10761–10770 (2012).
157. Almeida, A. S., Sonnewald, U., Alves, P. M. & Vieira, H. L. A. Carbon monoxide improves neuronal differentiation and yield by increasing the functioning and number of mitochondria. *J. Neurochem.* **138**, 423–435 (2016).
158. Kapetanaki, S. M. *et al.* A mechanism for CO regulation of ion channels. *Nat Commun* **9**, 907 (2018).
159. Zhang, R.-G., Yip, C.-Y. & Ko, W.-H. Regulation of Intracellular Calcium by Carbon Monoxide in Human Bronchial Epithelial Cells. *Cell Physiol Biochem* **42**, 2377–2390 (2017).
160. Elies, J. *et al.* Inhibition of the Cardiac Na⁺ Channel Nav1.5 by Carbon Monoxide. *Journal of Biological Chemistry* **289**, 16421–16429 (2014).
161. Hettiarachchi, N. T. *et al.* Peroxynitrite Mediates Disruption of Ca²⁺ Homeostasis by Carbon Monoxide via Ca²⁺ ATPase Degradation. *Antioxidants & Redox Signaling* **17**, 744–755 (2012).
162. Rana, N., McLean, S., Mann, B. E. & Poole, R. K. Interaction of the carbon monoxide-releasing molecule Ru(CO)₃Cl(glycinate) (CORM-3) with *Salmonella enterica* serovar Typhimurium: in situ measurements of carbon monoxide binding by integrating cavity dual-beam spectrophotometry. *Microbiology* **160**, 2771–2779 (2014).
163. Motterlini, R. Carbon monoxide-releasing molecules (CO-RMs): vasodilatory, anti-ischaemic and anti-inflammatory activities. *Biochemical Society Transactions* **35**, 1142–1146 (2007).
164. Romão, C. C., Blättler, W. A., Seixas, J. D. & Bernardes, G. J. L. Developing drug molecules for therapy with carbon monoxide. *Chem. Soc. Rev.* **41**, 3571 (2012).
165. Faizan, M. *et al.* CO-Releasing Materials: An Emphasis on Therapeutic Implications, as Release and Subsequent Cytotoxicity Are the Part of Therapy. *Materials* **12**, 1643 (2019).
166. Alberto, R. & Motterlini, R. Chemistry and biological activities of CO-releasing molecules (CORMs) and transition metal complexes. *Dalton Trans.* 1651 (2007) doi:10.1039/b701992k.
167. Pitchumony, T. S., Spingler, B., Motterlini, R. & Alberto, R. Syntheses, structural characterization and CO releasing properties of boranocarbonate [H₃BCO₂H]– derivatives. *Org. Biomol. Chem.* **8**, 4849 (2010).

168. Pitchumony, T. S., Spingler, B., Motterlini, R. & Alberto, R. Derivatives of Sodium Boranocarbonate as Novel CO-Releasing Molecules (CO-RMs). *CHIMIA* **62**, 277–279 (2008).
169. Motterlini, R., Mann, B. E. & Foresti, R. Therapeutic applications of carbon monoxide-releasing molecules. *Expert Opinion on Investigational Drugs* **14**, 1305–1318 (2005).
170. Kretschmer, R., Gessner, G., Görls, H., Heinemann, S. H. & Westerhausen, M. Dicarbonyl-bis(cysteamine)iron(II): A light induced carbon monoxide releasing molecule based on iron (CORM-S1). *Journal of Inorganic Biochemistry* **105**, 6–9 (2011).
171. Crook, S. H. *et al.* [Mn(CO)₄{S₂CNMe(CH₂CO₂H)}], a new water-soluble CO-releasing molecule. *Dalton Trans.* **40**, 4230 (2011).
172. Seixas, J. D. *et al.* Characterization of a versatile organometallic pro-drug (CORM) for experimental CO based therapeutics. *Dalton Trans.* **42**, 5985–5998 (2013).
173. Romanski, S. *et al.* Acyloxybutadiene tricarbonyl iron complexes as enzyme-triggered CO-releasing molecules (ET-CORMs): a structure–activity relationship study. *Dalton Trans.* **41**, 13862 (2012).
174. Yang, S. *et al.* Photo-activated CO-releasing molecules (PhotoCORMs) of robust sawhorse scaffolds [μ^2 -OOCR¹, η^1 -NH₂CHR²(C□O)OCH₃, Ru(I)₂CO₄]. *Dalton Trans.* **45**, 3727–3733 (2016).
175. Tavares, A. F. *et al.* The Bactericidal Activity of Carbon Monoxide–Releasing Molecules against *Helicobacter pylori*. *PLoS ONE* **8**, e83157 (2013).
176. Vieira, H. L. A., Queiroga, C. S. F. & Alves, P. M. Pre-conditioning induced by carbon monoxide provides neuronal protection against apoptosis: Carbon monoxide as neuroprotector. *Journal of Neurochemistry* **107**, 375–384 (2008).
177. Schallner, N. *et al.* Carbon Monoxide Abrogates Ischemic Insult to Neuronal Cells via the Soluble Guanylate Cyclase-cGMP Pathway. *PLoS ONE* **8**, e60672 (2013).
178. Almeida, A. S. *et al.* Improvement of neuronal differentiation by carbon monoxide: Role of pentose phosphate pathway. *Redox Biology* **17**, 338–347 (2018).
179. Almeida, A. S., Soares, N. L., Vieira, M., Gramsbergen, J. B. & Vieira, H. L. A. Carbon Monoxide Releasing Molecule-A1 (CORM-A1) Improves Neurogenesis: Increase of Neuronal Differentiation Yield by Preventing Cell Death. *PLoS ONE* **11**, e0154781 (2016).
180. Lin, C.-C., Yang, C.-C., Hsiao, L.-D., Chen, S.-Y. & Yang, C.-M. Heme Oxygenase-1 Induction by Carbon Monoxide Releasing Molecule-3 Suppresses Interleukin-1 β -Mediated Neuroinflammation. *Front. Mol. Neurosci.* **10**, 387 (2017).
181. Megías, J., Busserolles, J. & Alcaraz, M. J. The carbon monoxide-releasing molecule CORM-2 inhibits the inflammatory response induced by cytokines in Caco-2 cells: Anti-inflammatory effects of CORM-2 in Caco-2 cells. *British Journal of Pharmacology* **150**, 977–986 (2007).
182. Basuroy, S., Leffler, C. W. & Parfenova, H. CORM-A1 prevents blood-brain barrier dysfunction caused by ionotropic glutamate receptor-mediated endothelial oxidative stress and apoptosis. *American Journal of Physiology-Cell Physiology* **304**, C1105–C1115 (2013).
183. Fayad-Kobeissi, S. *et al.* Vascular and angiogenic activities of CORM-401, an oxidant-sensitive CO-releasing molecule. *Biochemical Pharmacology* **102**, 64–77 (2016).
184. Soares, N. L. & Vieira, H. L. A. Microglia at the Centre of Brain Research: Accomplishments and Challenges for the Future. *Neurochem Res* (2021) doi:10.1007/s11064-021-03456-1.
185. Bani-Hani, M. G., Greenstein, D., Mann, B. E., Green, C. J. & Motterlini, R. Modulation of Thrombin-Induced Neuroinflammation in BV-2 Microglia by Carbon Monoxide-Releasing Molecule 3. *J Pharmacol Exp Ther* **318**, 1315–1322 (2006).
186. Wilson, J. L. *et al.* Carbon monoxide reverses the metabolic adaptation of microglia cells to an inflammatory stimulus. *Free Radical Biology and Medicine* **104**, 311–323 (2017).

187. Dias-Pedroso, D. *et al.* Carbon Monoxide-Neuroglobin Axis Targeting Metabolism Against Neuroinflammation. <https://www.researchsquare.com/article/rs-852619/v1> (2021) doi:10.21203/rs.3.rs-852619/v1.
188. Scheiblich, H. & Bicker, G. Regulation of microglial migration, phagocytosis, and neurite outgrowth by HO-1/CO signaling: Effects of CO on Microglial Activity. *Devel Neurobio* **75**, 854–876 (2015).
189. Schallner, N. *et al.* Microglia regulate blood clearance in subarachnoid hemorrhage by heme oxygenase-1. *J. Clin. Invest.* **125**, 2609–2625 (2015).
190. Kaiser, S., Selzner, L., Weber, J. & Schallner, N. Carbon monoxide controls microglial erythrophagocytosis by regulating CD36 surface expression to reduce the severity of hemorrhagic injury. *Glia* **glia.23864** (2020) doi:10.1002/glia.23864.
191. Lee, S. *et al.* Carbon Monoxide Confers Protection in Sepsis by Enhancing Beclin 1-Dependent Autophagy and Phagocytosis. *Antioxidants & Redox Signaling* **20**, 432–442 (2014).
192. Chen, L. *et al.* Carbon monoxide alleviates senescence in diabetic nephropathy by improving autophagy. *Cell Prolif* **54**, (2021).
193. Coughlan, M. P. The role of molybdenum in human biology. *J Inherit Metab Dis* **6**, 70–77 (1983).
194. Novotny, J. A. & Turnlund, J. R. Molybdenum Intake Influences Molybdenum Kinetics in Men. *The Journal of Nutrition* **137**, 37–42 (2007).
195. Aires, I. D. *et al.* Blockade of microglial adenosine A_{2A} receptor suppresses elevated pressure-induced inflammation, oxidative stress, and cell death in retinal cells. *Glia* **67**, 896–914 (2019).
196. Champion, J. A., Walker, A. & Mitragotri, S. Role of Particle Size in Phagocytosis of Polymeric Microspheres. *Pharm Res* **25**, 1815–1821 (2008).
197. Majerova, P. *et al.* Microglia display modest phagocytic capacity for extracellular tau oligomers. *J Neuroinflammation* **11**, 161 (2014).
198. Ebert, S. *et al.* Chondroitin sulfate disaccharide stimulates microglia to adopt a novel regulatory phenotype. *Journal of Leukocyte Biology* **84**, 736–740 (2008).
199. Cunha, C., Gomes, C., Vaz, A. R. & Brites, D. Exploring New Inflammatory Biomarkers and Pathways during LPS-Induced MI Polarization. *Mediators of Inflammation* **2016**, 1–17 (2016).
200. Kobayashi, Y. *et al.* Lipopolysaccharides Derived from *Pantoea* agglomerans Can Promote the Phagocytic Activity of Amyloid β in Mouse Microglial Cells. *AR* **37**, (2017).
201. Shiratsuchi, A., Watanabe, I., Takeuchi, O., Akira, S. & Nakanishi, Y. Inhibitory Effect of Toll-Like Receptor 4 on Fusion between Phagosomes and Endosomes/Lysosomes in Macrophages. *J Immunol* **172**, 2039–2047 (2004).
202. Kim, H. J. *et al.* Carbon monoxide-induced TFEB nuclear translocation enhances mitophagy/mitochondrial biogenesis in hepatocytes and ameliorates inflammatory liver injury. *Cell Death Dis* **9**, 1060 (2018).
203. Joe, Y. *et al.* Cross-talk between CD38 and TTP Is Essential for Resolution of Inflammation during Microbial Sepsis. *Cell Reports* **30**, 1063-1076.e5 (2020).
204. Riquelme, S. A., Pogu, J., Anegon, I., Bueno, S. M. & Kalergis, A. M. Carbon monoxide impairs mitochondria-dependent endosomal maturation and antigen presentation in dendritic cells: Antigen processing. *Eur. J. Immunol.* **45**, 3269–3288 (2015).
205. Campbell, N. K. *et al.* Naturally derived Heme-Oxygenase 1 inducers attenuate inflammatory responses in human dendritic cells and T cells: relevance for psoriasis treatment. *Sci Rep* **8**, 10287 (2018).
206. Nakahira, K. *et al.* Carbon monoxide differentially inhibits TLR signaling pathways by regulating ROS-induced trafficking of TLRs to lipid rafts. *Journal of Experimental Medicine* **203**, 2377–2389 (2006).

